



# Non-universal SUSY models, $g_\mu - 2$ , $m_H$ and dark matter

John Ellis<sup>1,2</sup>, Keith A. Olive<sup>3</sup>, Vassilis C. Spanos<sup>3,4,a</sup>

<sup>1</sup> Theoretical Particle Physics and Cosmology Group, Department of Physics, King's College London, London WC2R 2LS, UK

<sup>2</sup> Theoretical Physics Department, CERN, 1211, Geneva 23, Switzerland

<sup>3</sup> William I. Fine Theoretical Physics Institute, School of Physics and Astronomy, University of Minnesota, Minneapolis, MN 55455, USA

<sup>4</sup> Section of Nuclear and Particle Physics, Department of Physics, National and Kapodistrian University of Athens, 157 84 Athens, Greece

Received: 22 July 2024 / Accepted: 12 October 2024 / Published online: 28 October 2024  
© The Author(s) 2024

**Abstract** We study the anomalous magnetic moment of the muon,  $g_\mu - 2 \equiv 2a_\mu$ , in the context of supersymmetric models beyond the CMSSM, where the unification of either the gaugino masses  $M_{1,2,3}$  or sfermion and Higgs masses is relaxed, taking into account the measured mass of the Higgs boson,  $m_H$ , the cosmological dark matter density and the direct detection rate. We find that the model with non-unified gaugino masses can make a contribution  $\Delta a_\mu \sim 20 \times 10^{-10}$  to the anomalous magnetic moment of the muon, for example if  $M_{1,2} \sim 600$  GeV and  $M_3 \sim 8$  TeV. The model with non-universal sfermion and Higgs masses can provide even larger  $\Delta a_\mu \sim 24 \times 10^{-10}$  if the sfermion masses for the first and the second generations are  $\sim 400$  GeV and that of the third is  $\sim 8$  TeV. We discuss the prospects for collider searches for supersymmetric particles in specific benchmark scenarios illustrating these possibilities, focusing in particular on the prospects for detecting the lighter smuon and the lightest neutralino.

## 1 Introduction

It has been more than two decades since the initial report of a deviation,  $\Delta a_\mu$  between the experimental measurement of the muon anomalous magnetic moment  $g_\mu - 2 \equiv 2a_\mu$  and the Standard Model theoretical prediction [1]. The significance of this “anomalous anomaly” grew over time with the enhanced precision of the BNL experiments [2] and the recent measurements from the Fermilab experiment [3]. On the theory side, the data-driven Standard Model theoretical predictions were refined, thanks to better estimations of the hadronic vacuum polarization and light-by-light scattering effects [4]. The combined BNL and Fermilab results yield [5, 6]

$$a_\mu^{exp} = 116592059(22) \times 10^{-11} \quad (1)$$

whereas the data-driven theoretical value is [4]

$$a_\mu^{th} = 116591810(43) \times 10^{-11}, \quad (2)$$

corresponding to a discrepancy of  $\Delta a_\mu = (24.9 \pm 4.8) \times 10^{-10}$ .

However, the uncertainties in first-principles lattice calculations have now been reduced to a level comparable to the data-driven calculation. Moreover, a pioneering lattice calculation of the intermediate-scale “window function” [7], when extrapolated to larger and smaller scales, yielded a central value of  $a_\mu$  that is in significant tension with the data-driven estimate and corresponds to a smaller discrepancy of  $\Delta a_\mu = (10.7 \pm 6.9) \times 10^{-10}$ . Subsequently, several other lattice calculations [8] of the window function have yielded numerical results that are similar to those of [7].

More recently, the CMD-3 Collaboration has published new  $e^+e^- \rightarrow 2\pi$  production data [9] in the energy range  $E_{CM} < 1$  GeV that are in significant tension with the previous world average results used in [4], and correspond to an even smaller discrepancy of  $\Delta a_\mu = (4.9 \pm 5.5) \times 10^{-10}$ . This has led a reappraisal of previous results on  $e^+e^- \rightarrow 2\pi$  production and of estimates of the low-energy vacuum polarization using  $\tau \rightarrow \nu + \text{hadrons}$  data, leading to an estimated discrepancy of  $\Delta a_\mu = (12.3 \pm 4.9) \times 10^{-10}$  [10]. Another new development has been a high-precision lattice calculation of the hadronic vacuum polarization combined with an estimate of the long-distance contribution based on low-energy experiments that yields  $\Delta a_\mu = (4.0 \pm 4.4) \times 10^{-10}$  [11].

Figure 1 displays the estimates of  $\Delta a_\mu$  introduced above: the data-driven estimate [4], the lattice calculation in [7], the estimate based on the recent CMD-3 experimental measurement [9], and the experimental re-evaluation in [10].

<sup>a</sup> e-mail: [vspanos@phys.uoa.gr](mailto:vspanos@phys.uoa.gr) (corresponding author)

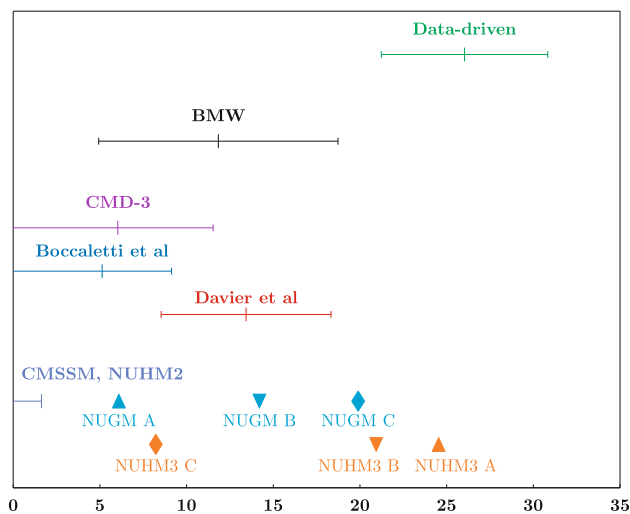


**Fig. 1** Comparison of experimental and theoretical estimates of  $\Delta a_\mu$  [4, 7, 9, 10], in  $10^{-10}$  units, with calculations in supersymmetric models including the benchmarks introduced in this paper

Following the initial BNL experimental result, theories based on supersymmetry were quickly suggested as explanations for the apparent discrepancy between experiment and the data-driven theoretical calculations within the Standard Model [12–22]. These calculations motivated light smuon and neutralino masses of a few hundred GeV. However, the enthusiasm for supersymmetric theories has diminished subsequently, as direct evidence for supersymmetry has remained elusive, particularly in the Large Hadron Collider (LHC) experiments [23]. When the LHC results are interpreted within the Constrained Minimal Supersymmetric extension of the Standard Model (CMSSM), in which all the gaugino masses and all the sfermion masses are assumed to be universal at some high unification scale, the possible supersymmetric contribution to  $a_\mu$  is constrained to be much smaller [24–37] than the discrepancy between the experimental data and the data-driven theoretical estimate recommended in [4], as seen in Fig. 1.

However, for several reasons the comparison between supersymmetric models and the data merits a more thorough study. First, the new lattice calculations and data on the hadron vacuum polarization suggest that the discrepancy between experimental data and the Standard Model may be smaller than thought previously. Secondly, there are many possible generalizations of the CMSSM that could accommodate a light smuon and a light neutralino mass simultaneously with the heavier squarks and gluinos indicated by the unsuccessful LHC searches. Thirdly, the lower limits on sparticle masses set in simplified models often do not apply to more general models see, e.g., [38].

We show in this paper that a significant supersymmetric contribution to  $a_\mu$  that could match any of the estimates of the discrepancy between the Standard Model and the BNL

and Fermilab measurements mentioned above, i.e.,  $\Delta a_\mu \sim (25, 10 \text{ or } 5) \times 10^{-10}$  if the specific unification conditions on the gaugino and/or sfermion masses are relaxed. We illustrate this point within two specific generalizations of the CMSSM, one in which the gaugino masses  $M_{1,2,3}$  are non-universal [37, 39, 40] (the NUGM), and one in which unification of the masses of the first- and second-generation sfermions, the third-generation sfermions and the Higgs scalar multiplets is relaxed [41] (the NUHM3). In both cases, we perform an extensive scan of the parameter space using Markov Chain Monte Carlo (MCMC) techniques similar to those used previously to scan the CMSSM parameter space [42], which are geared to providing a Higgs mass and relic density for the lightest supersymmetric particle (LSP) compatible with experimental constraints [43–46]. We also highlight benchmark scenarios that illustrate the phenomenological possibilities, taking into account also calculations of the mass of the Higgs boson,  $m_H$ , and constraints on the density of relic cold dark matter and its possible spin-independent and -dependent cross-sections for scattering on matter.

The values of  $\Delta a_\mu$  attainable in the NUGM and NUHM3 are illustrated by these benchmark scenarios, as indicated in Fig. 1. As shown there, we find that a model with non-universal gaugino masses (the NUGM) can yield  $\Delta a_\mu \sim 20 \times 10^{-10}$ , sufficient to accommodate the lattice and CMD-3 results, e.g., if  $M_{1,2} \sim 600$  GeV and  $M_3 \sim 8$  TeV. In the case of non-universal sfermion and Higgs masses (the NUHM3), we find that even larger  $\Delta a_\mu \sim 24 \times 10^{-10}$  can be reached, sufficient to accommodate the data-driven value given in [4], for first- and second-generation sfermion masses  $\sim 400$  GeV and third-generation sfermion masses  $\sim 8$  TeV. The Planck [46] value of the cosmological dark matter density can be saturated by the LSP density in the NUGM, but not in the NUHM3 because the spin-independent dark matter scattering cross section is larger in that model.

The paper is organized as follows. In Sect. 2 we introduce the NUGM and NUHM3 models that we study, and in Sect. 3 we describe our analysis procedure. Our results are presented in Sect. 4: those for the NUGM in Sect. 4.1 and those for the NUHM3 in Sect. 4.2. Section 5 focuses on some benchmark scenarios that illustrate the phenomenological possibilities in these models, including the possibilities for probing them at the LHC and elsewhere, as well as their possible contributions to  $a_\mu$ . Finally, Sect. 6 summarizes our conclusions.

## 2 The models

As already mentioned, it is well known that a substantial discrepancy between the Standard Model and experimental measurements of the anomalous magnetic moment of the muon  $g_\mu - 2$  can no longer be explained within the CMSSM [24–34, 36, 37, 40, 41]. The models considered here

are based on generalizations of the CMSSM [47–63], which is defined by four continuous parameters: a universal gaugino mass,  $M_{1/2}$ , a universal scalar mass,  $m_0$ , a universal trilinear mass,  $A_0$  (all three of which are supersymmetry-breaking mass terms) and the ratio of the vacuum expectation value (vev) of the neutral components of the Higgs doublets  $\langle H_2^0 \rangle / \langle H_1^0 \rangle = \tan \beta$ . In addition there is the freedom to choose the sign of the  $\mu$ -term. The leading supersymmetric contributions to  $g_\mu - 2$  arise from two one-loop graphs: one involving charginos and sneutrinos and another that involves smuons and neutralinos.<sup>1</sup> Our calculations of the contributions to  $g_\mu - 2$  are detailed in [12] and follow the calculations in [65]. Substantial contributions to  $g_\mu - 2$  may arise if either the chargino/neutralino pair and/or the smuon/neutralino pair weigh a few hundred GeV. However, in the CMSSM the Higgs mass  $m_H = 125$  GeV in conjunction with the constraints on direct detection of astrophysical dark matter put severe lower limits on both the assumed universal gaugino mass  $M_{1/2}$  and the common sfermion mass  $m_0$ , implying  $m_0 \geq 10$  TeV and  $M_{1/2} \geq 4 - 5$  TeV [42]. These limits imply that in the CMSSM all sleptons and gauginos are heavy, and consequently the supersymmetric contributions to  $g_\mu - 2$  are small, as we review below.

However, if one relaxes either the gaugino [37, 39, 40] or the sfermion [41] mass unification conditions, one may expect to find enhanced supersymmetric corrections to  $g_\mu - 2$ . With this in mind, we explore two extensions of the CMSSM in which these mass unification conditions are relaxed:

- **Non-Universal gaugino masses:** A model in which gaugino mass unification is abandoned (NUGM) [37, 39, 40, 66–76], which has six free parameters, namely separate gaugino masses  $M_1, M_2, M_3$  in addition to the other CMSSM parameters,  $m_0, A_0, \tan \beta$  and  $sgn(\mu)$ .
- **Non-universal sfermion and Higgs masses:** Two well studied extensions of the CMSSM allow for either one [77–79] or both [80–85] of the Higgs soft mass parameters to differ from the universal scalar masses. These are known as the NUHM1 and NUHM2, respectively, with  $m_{H_1} = m_{H_2} \neq m_0$  or  $m_{H_1} \neq m_{H_2} \neq m_0$ . The extension we study here (dubbed NUHM3 [41]) is a model in which common masses of the first and second sfermion generations,  $m_{012}$ , differ from that of the third,  $m_{03}$ , and those of the two Higgs multiplets,  $m_{H_1}$  and  $m_{H_2}$ , at the GUT scale. It is convenient to use the minimization conditions of the effective electroweak potential to trade  $m_{H_1, H_2}$  for the Higgsino mixing parameter  $\mu$  and the mass of the pseudoscalar Higgs boson  $A, M_A$ . The replacement of  $m_{H_1, H_2}$  by  $\mu, M_A$  is the same as in the non-universal Higgs model (NUHM2) or a general two Higgs doublet

model (2HDM). This model is characterized by seven parameters:  $M_{1/2}, m_{012}, m_{03}, \mu, M_A, A_0$  and  $\tan \beta$ . Since the sign of the Higgsino mixing parameter  $\mu$  is the same as that of the supersymmetric contribution to  $g_\mu - 2$ , we consider only positive values for this parameter.

A related study [86] was performed allowing for non-universal gaugino masses and non-universal Higgs masses, with eight free continuous parameters. Models attempting to account for  $\Delta a_\mu$  for which the relic density is determined by stau coannihilation [87–95] were considered in [96–98] or by a well-tempered neutralino [99, 100] in [101]. Better agreement between theory and experiment was also seen a CMSSM-like model based on Flipped SU(5) $\times$ U(1) [35, 36]. This is partially due to the additional freedom of additional input parameters, and it was shown there, that non-Universal boundary conditions are needed to obtain a sizable contribution to  $\Delta a_\mu$ . Even more generalized models form the basis of the pMSSM [38, 102–117].

### 3 Analysis procedure

We use the SSARD code [118] to compute the particle mass spectrum and relic density. This code incorporates the two-loop running of the input soft supersymmetry-breaking parameters from the input scale  $M_{\text{GUT}}$  (defined as the scale where the electroweak gauge couplings  $g_1$  and  $g_2$  meet) down to the electroweak scale, identified with  $m_Z$ . In the CMSSM and NUGM, the  $\mu$  parameter is extracted by minimizing the one-loop corrected effective potential [119] at the scale  $m_Z$ , while the pseudoscalar Higgs mass  $M_A$  is computed using the results of [120]. The radiative corrections to the light Higgs boson mass  $m_H$  are computed with the FeynHiggs code [121–129]. We also include the full one-loop corrections to the physical chargino and neutralino masses calculated in [130–132].

We have scanned the six-dimensional parameter space of the NUGM and the seven-dimensional parameter space of the NUHM3 with MCMC routines using the likelihood functions as defined in Eq. (3) below, for the following three basic predictions of the model: the Higgs mass,  $m_H$ , the neutralino relic density,  $\Omega_\chi h^2$ , and the muon dipole moment,  $g_\mu - 2$ . The likelihood functions are fixed by the following experimental ranges:  $m_H = 125 \pm 2$  GeV,  $\Omega_\chi h^2 = 0.12 \pm 0.0012$  and  $\Delta a_\mu = (24.9 \pm 4.8) \times 10^{-10}$ . These ranges are chosen to aid the parameter scan, but do not directly affect our results.<sup>2</sup> The range of  $m_H$  is much larger than the experimental uncertainty,

<sup>1</sup> See [64] for the two-loop corrections, which are subdominant.

<sup>2</sup> The  $3\sigma$  uncertainty we adopt for  $\Omega_\chi h^2$  is broad enough to account for theoretical uncertainties in its calculation. However, in the phenomenological analysis of the models, we also consider a sample of points where the value  $\Omega_\chi h^2 = 0.1236$  is used as an upper limit.

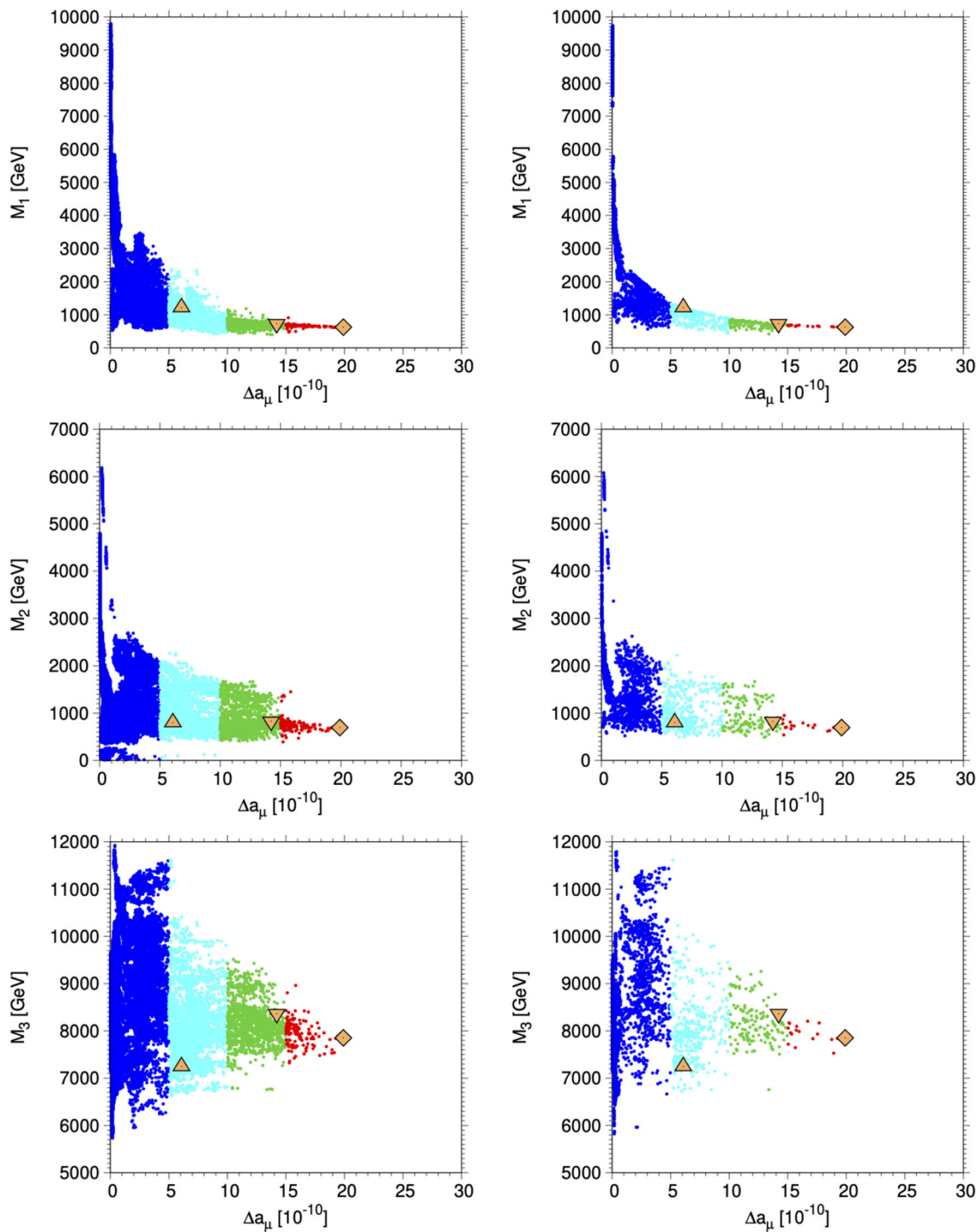


**Fig. 2** Allowed values of the gaugino masses  $M_{1,2,3}$  in the NUGM as functions of  $\Delta a_\mu$ . The left panels are for  $\Omega_\chi h^2 \leq 0.1236$ , whereas the right panels are for points with  $0.1164 \leq \Omega_\chi h^2 \leq 0.1236$ . The yellow symbols indicate the locations of the NUGM benchmark points discussed in Sect. 5 below

and is also broader than the current estimated uncertainty in MSSM calculations. However, it is consistent at  $2\sigma$  with the theoretical uncertainty in the calculation of  $m_H$  using FeynHiggs [121–129], which we adopt in all the results below.

Each likelihood function is defined as

$$\mathcal{L}_O = e^{-\chi_O^2/2}, \quad \text{where } \chi_O^2 = \left(\frac{\mathcal{O}_{\text{th}} - \mathcal{O}_{\text{ex}}}{\sigma}\right)^2, \quad (3)$$

with  $\mathcal{O} = \{\Delta a_\mu, m_H, \Omega_\chi h^2\}$ . For each observable,  $\mathcal{O}_{\text{th}}$  represents its value as calculated in our code,  $\mathcal{O}_{\text{ex}}$  is its

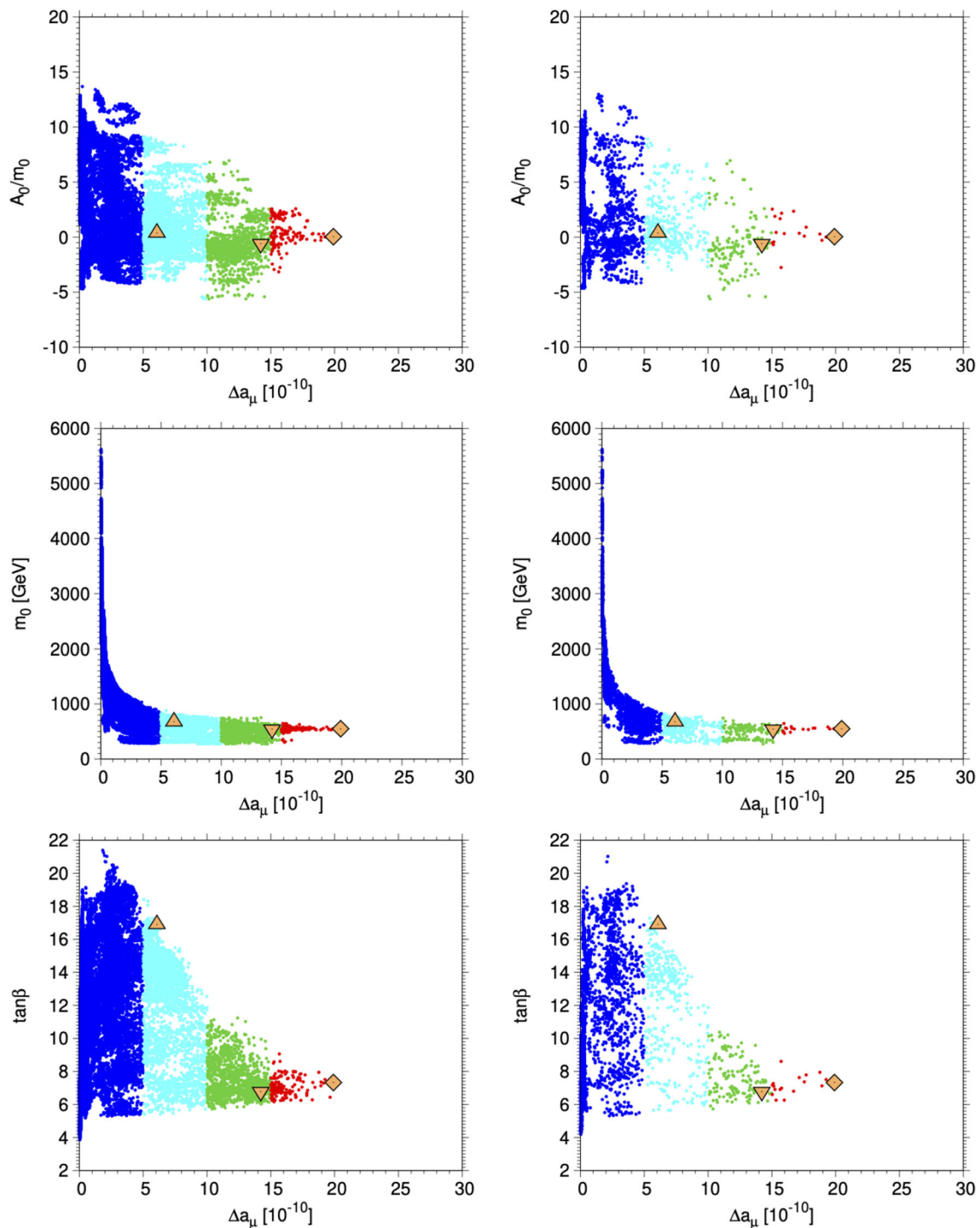


**Fig. 3** As in Fig. 2, showing the allowed values of  $A_0/m_0$ ,  $m_0$  and  $\tan\beta$  in the NUGM as functions of  $\Delta a_\mu$

current experimental value, and  $\sigma$  is the corresponding uncertainty. The total likelihood is defined as the product of these three likelihoods. We then use this combined likelihood to run the MCMC code, which is based on a Metropolis–Hastings [133, 134] routine. This MCMC code is primarily used to increase the efficiency of our scans, as done in [42],

and is not used for a statistical interpretation of the points presented in our figures.

We present results assuming that  $\Omega_\chi h^2$  either provides all of the cosmological cold dark matter density [46], or that there is potentially another contribution to the cold dark matter density. Likewise, motivated by the recent lattice and

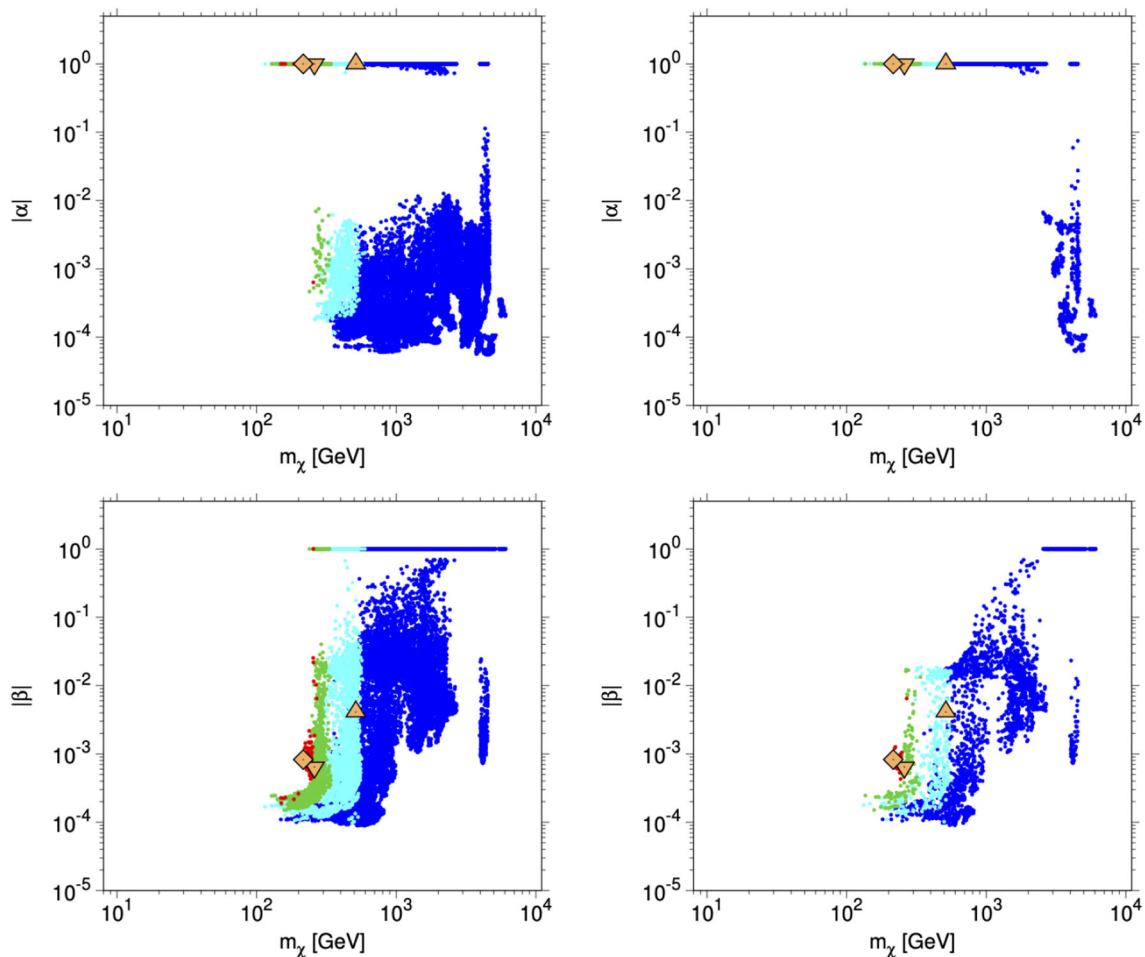


**Fig. 4** The Bino (upper panels) and Wino (lower panels) components  $\alpha$  and  $\beta$ , respectively, of the LSP for the NUGM points shown in Fig. 2 as functions of  $m_\chi$ . The color coding corresponds to the values of  $\Delta a_\mu$  shown in Fig. 2

experimental results, we consider the possibility that  $\Delta a_\mu$  is smaller than the range quoted above.

We assume that the lightest neutralino is the lightest supersymmetric particle (LSP), and that  $R$ -parity is conserved, so that the LSP is stable. We apply the same accelerator constraints as in [36], namely:

- The LEP experiments' exclusion of charginos lighter than 103 GeV if  $m_{\tilde{\chi}^\pm} - m_\chi \geq 3$  GeV [135] and  $m_{\tilde{\chi}^\pm} > 91.9$  GeV for  $m_{\tilde{\chi}^\pm} - m_\chi < 3$  GeV [136].
- In both the models we study, the smuon and selectron masses are equal up to small corrections related to the muon-electron mass difference. The LEP experiments established lower limits on selectron masses that are generally stronger than those on smuons, and stronger for left-handed sleptons. For our purposes the most relevant LEP slepton constraints are those on  $m_{\tilde{e}_R}$ , which also depend on other sparticle masses, in particular  $m_\chi$  [137]. We use a LEP lower limit of 100 GeV in general, reducing to 73 GeV if  $m_{\tilde{\mu}_R} - m_\chi \lesssim 2$  GeV.
- At the LHC, ATLAS has established the lower limit  $m_{\tilde{\mu}} \gtrsim 700$  GeV when  $m_\chi = 0$ , falling to  $\gtrsim 600$  GeV when  $m_\chi \simeq 400$  GeV [138]. At lower smuon masses there is an allowed corridor where  $m_{\tilde{\mu}} - m_\chi \lesssim 100$  GeV that extends down to the LEP lower limit on  $m_{\tilde{\mu}}$ . We have implemented fully these LHC limits in our scan of the sparticle parameter space: see [139] for a full description.
- An additional LHC constraint is relevant for compressed spectra when  $m_{\mu_R} - m_\chi \lesssim 15$  GeV [140], which is maximized when  $m_{\tilde{\mu}_R} - m_\chi \simeq 10$  GeV, in which case it excludes  $m_{\tilde{\mu}_R} \lesssim 150$  GeV.
- We do not impose a priori LHC constraints on heavier sparticles that are, in general, more model-dependent. (See, in particular [38].) However, we do comment *a posteriori* on their potential significances for benchmark NUGM and NUHM3 scenarios.
- As noted earlier, the Higgs mass is constrained to lie in the range  $123 \text{ GeV} \leq m_H \leq 127 \text{ GeV}$  as computed using FeynHiggs [121–129].

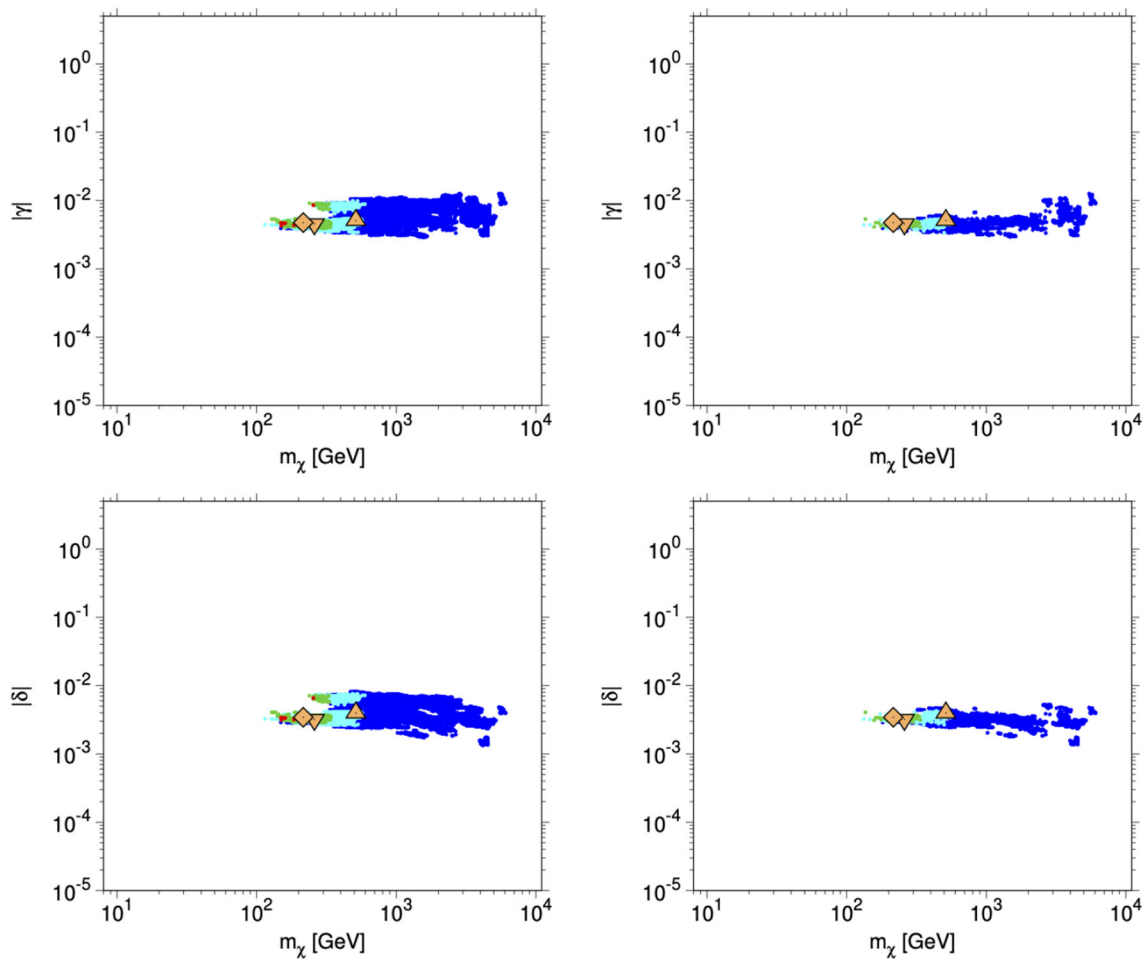


**Fig. 5** The Higgsino components  $\gamma$  and  $\delta$ , respectively, of the LSP for the NUGM points shown in Fig. 2 as functions of  $m_\chi$ . The color coding corresponds to the values of  $\Delta a_\mu$  shown in Fig. 2

- For cases where the LSP makes up all of the cold dark matter density, we require  $\Omega_\chi h^2 = 0.1200 \pm 0.0036$  which represents the  $3\sigma$  range as determined by Planck [46]. When the LSP is allowed to make up only a fraction of the dark matter, we simply exclude models which produce  $\Omega_\chi h^2 > 0.1236$ .

We also compute in our analysis the spin-dependent and -independent cross sections for the scattering of the LSP on protons. For a description of our calculations of these, see [141, 142]. The resulting cross sections are compared to the recent results from LZ [143] for the spin-independent scattering cross section and PICO [144] for the spin-dependent scattering cross section on protons. Note that while we exclude input parameters which yield a relic density in excess of the Planck determination, we do not exclude *a priori* points that yield a scattering cross section in excess of the current experimental limits, but comment *a posteriori* on their impacts on the NUGM and NUHM3 parameter spaces.

## 4 Results

### 4.1 Non-universal gaugino mass model (NUGM)

As described above, the NUGM is characterized by six parameters. In all cases, we have chosen  $\mu > 0$ . In our scan of the parameter space, we have covered the following ranges

$$\begin{aligned}
 M_1 &= 0 - 10 \text{ TeV}, \\
 M_2 &= 0 - 10 \text{ TeV}, \\
 M_3 &= 0 - 15 \text{ TeV}, \\
 m_0 &= 0 - 10 \text{ TeV}, \\
 |A_0/m_0| &= 0 - 40, \\
 \tan \beta &= 1 - 50.
 \end{aligned}
 \tag{4}$$

The supersymmetry-breaking mass parameters are input at the GUT scale, taken to be where the two electroweak gauge couplings are unified, and run down to the electroweak scale. Any set of inputs that do not yield a neutralino LSP is dis-

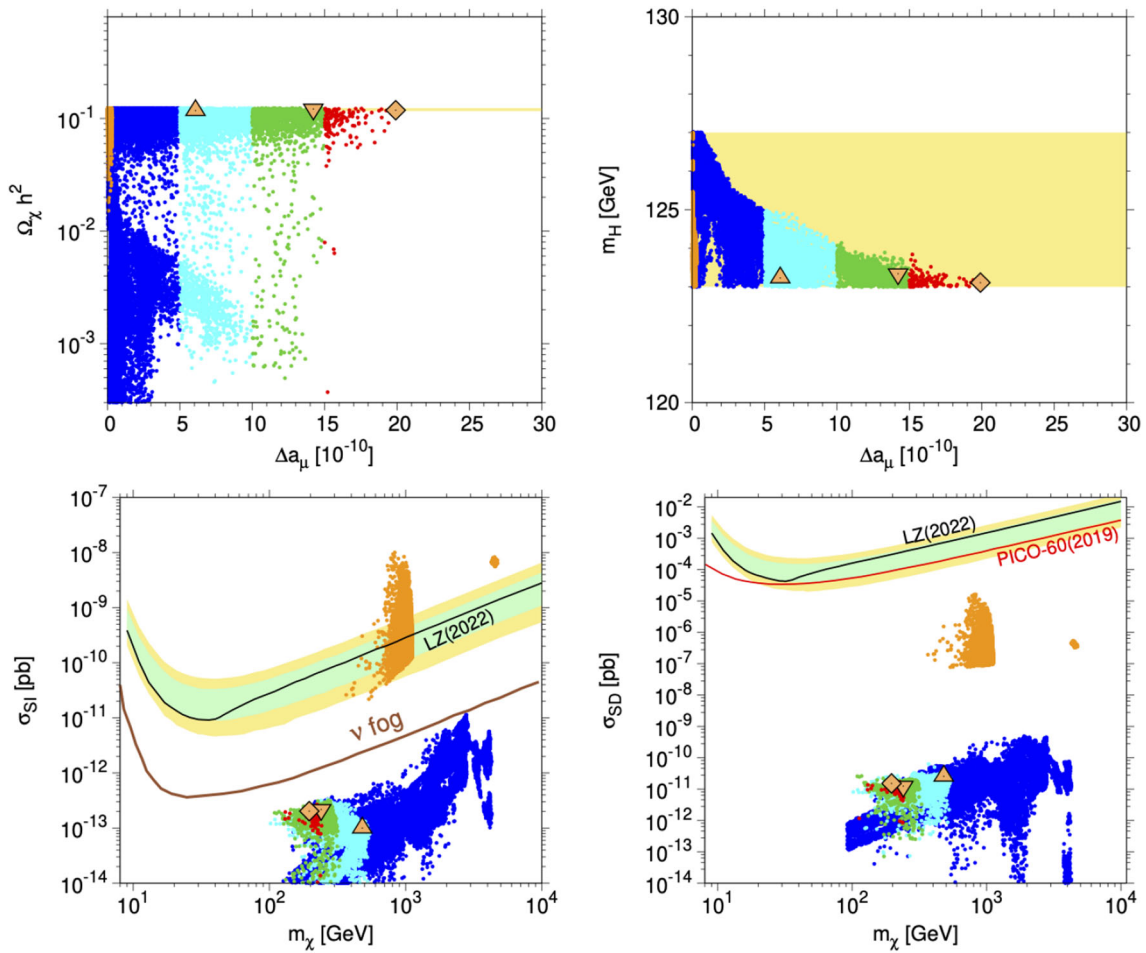


**Fig. 6** Scatter plots of projections of the results for the NUGM from MCMC runs with non-universal  $M_{1,2,3}$  but universal  $m_0$  and  $A_0$ . These parameters and  $\tan \beta$  are allowed to vary over the ranges given in Eq. (4). We show the relic LSP density,  $\Omega_\chi h^2$  (top left); the Higgs mass,  $m_H$  (top right); the spin-independent (SI)  $\chi - p$  scattering cross section,  $\sigma_{SI}$  (lower left) and the spin-dependent (SD)  $\chi - p$  scattering cross section,

$\sigma_{SD}$  (lower right). Points in these panels were selected by imposing only the upper limit to the LSP density  $\Omega_\chi h^2 \leq 0.1236$ . The direct detection cross sections are re-scaled by a factor  $\Omega_\chi h^2 / 0.12$ . The orange points correspond to a sample with unified gaugino masses (the CMSSM). The other colors correspond to the different  $5 \times 10^{-10}$  ranges of  $\Delta a_\mu$ . The neutrino fog layer [156] for SI scattering is indicated by a brown line

carded. In addition, we discard parameter choices that lead to a tachyonic Higgs pseudoscalar or do not satisfy the electroweak symmetry breaking minimization conditions, i.e., that lead to  $\mu^2 < 0$ .<sup>3</sup>

In our scan of the six-dimensional parameter space of the NUGM we obtain 250,000 points from the MCMC code. About 60,000 of them pass the kinematical constraints described in Sect. 3 and satisfy the requirement that LSP is the lightest neutralino. Of these, 45,000 points satisfy the Higgs boson mass bound  $m_H = 125 \pm 2$  GeV and the relic density requirement  $\Omega_\chi h^2 \leq 0.1236$ . Of these, 3,000 points yield an

LSP density within the Planck  $3\sigma$  range for the overall cold dark matter density:  $0.1164 \leq \Omega_\chi h^2 \leq 0.1236$ .

In Figs. 2 and 3 we show the values of the input parameters for points that survive all of the constraints discussed in the previous Section. The values are displayed as functions of the calculated value of  $\Delta a_\mu$  for each point and color-coded in intervals of  $\Delta a_\mu = 5 \times 10^{-10}$ . Plots on the left use only the upper bound on  $\Omega_\chi h^2$ , whereas those on the right are restricted to the Planck determination of the cold dark matter density, as indicated in the caption. As might be expected, we see in Fig. 2 that the viable resulting parameter sets indicate that  $M_1 \sim M_2 \lesssim 1$  TeV for points with the largest contribution to  $\Delta a_\mu \sim 20 \times 10^{-10}$ . However, the gluino mass  $M_3 \sim 8$  TeV is significantly larger, as is required in order to increase the stop mass sufficiently to obtain a Higgs mass consistent with experiment. The yellow

<sup>3</sup> We also made an exploratory scan with negative values of  $M_i$ . Changing the sign of  $M_1$  flips the sign of  $\Delta a_\mu$ , which can be compensated by choosing  $\mu < 0$ . We checked that there were no qualitative effects on our results for  $M_{2,3}$ . Therefore in all that follows, we choose to keep  $M_i > 0$  and  $\mu > 0$ .

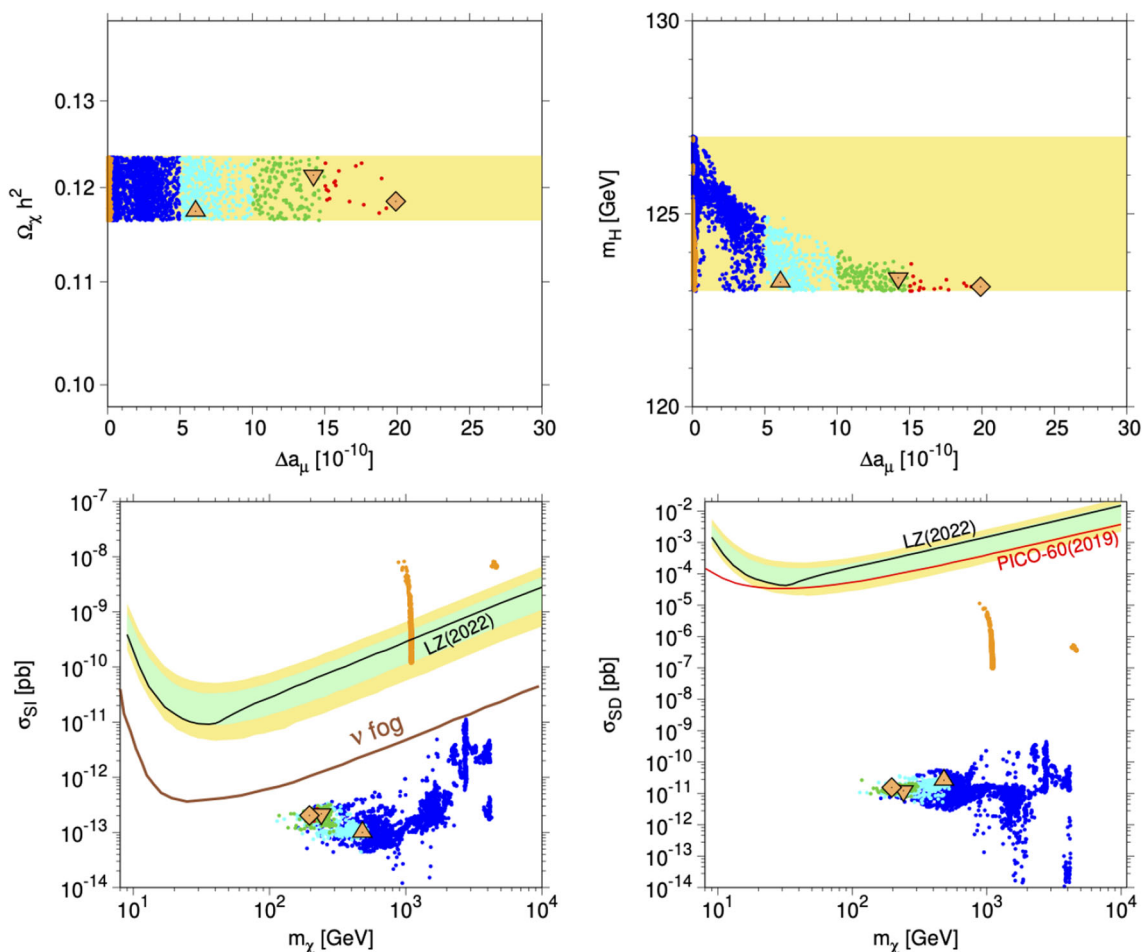


**Fig. 7** As in Fig. 6, but restricting the LSP density to the preferred cosmological range  $0.1164 \leq \Omega_\chi h^2 \leq 0.1236$

symbols in these and subsequent planes indicate the locations of the NUGM benchmark points discussed in Sect. 5 below.

We see in the top panels of Fig. 3 that the least well determined input parameter is  $A_0/m_0$ , for which no specific value is indicated. Indeed,  $A_0/m_0$  is only very weakly constrained for points that yield small values of  $\Delta a_\mu \lesssim 5 \times 10^{-10}$ , whereas relatively small values of  $|A_0/m_0| \lesssim 2$  are favored for points that yield larger values of  $\Delta a_\mu \gtrsim 15 \times 10^{-10}$ . The middle panels of Fig. 3 show, unsurprisingly, that larger values of  $\Delta a_\mu$  are correlated with smaller values of  $m_0$ . This preference for  $m_0 \sim 0.5$  TeV enables a suitably low value of  $m_{\tilde{\mu}}$  to be obtained. The bottom panels of Fig. 3 show that, whereas small values of  $\Delta a_\mu \lesssim 5 \times 10^{-10}$  are possible for values of  $\tan \beta \in [4, 20]$ , large values of  $\Delta a_\mu \gtrsim 15 \times 10^{-10}$  are found only for  $\tan \beta \sim 8$ .

To understand this, we recall that in order to get a sizeable contribution to  $\Delta a_\mu$ , a light smuon and LSP are preferred, so a typical acceptable NUGM point has small  $M_1, M_2$  and  $m_0$ . On the other hand, high values of  $M_3$  are needed in order to obtain heavy stops that yield a Higgs mass in the required region  $125 \pm 2$  GeV. One then finds that the two-loop RGEs

affect  $m_{H_{1,2}}$  and increase  $\mu$  which drives  $m_{\tilde{\mu}_L}$  and  $m_{\tilde{\tau}_1}$  lighter for higher  $M_3$ , favoring the stau coannihilation region, where  $\Omega_\chi h^2 \simeq 0.12$ . At  $M_3 \gtrsim 8$  TeV, the stau becomes the LSP and ultimately tachyonic. Similarly,  $\tan \beta$  must be  $\lesssim 10$ , since higher values also result in a stau LSP.

The composition of the neutralino LSP,  $\chi$ , can be expressed as a linear combination of the Bino (U(1) gaugino), neutral Wino (SU(2) gaugino), and two neutral Higgsinos

$$\chi = \alpha \tilde{B} + \beta \tilde{W}^3 + \gamma \tilde{H}_1^0 + \delta \tilde{H}_2^0, \tag{5}$$

whose masses and hence the neutralino composition are determined by the gaugino masses,  $M_{1,2}$ , the  $\mu$  parameter and  $\tan \beta$ . Figure 4 displays the gaugino contents,  $\alpha$  and  $\beta$ , of the NUGM sample points. We see that they mainly exhibit two possibilities: an almost pure Bino with a small admixture of the neutral Wino, or vice versa. The points are color-coded according to their values of  $\Delta a_\mu$  as in Fig. 2. We note that the majority of the points with relatively large  $\Delta a_\mu \gtrsim 15 \times 10^{-10}$  have a dominant Bino component. The most significant difference between the left panels (where the Planck range of

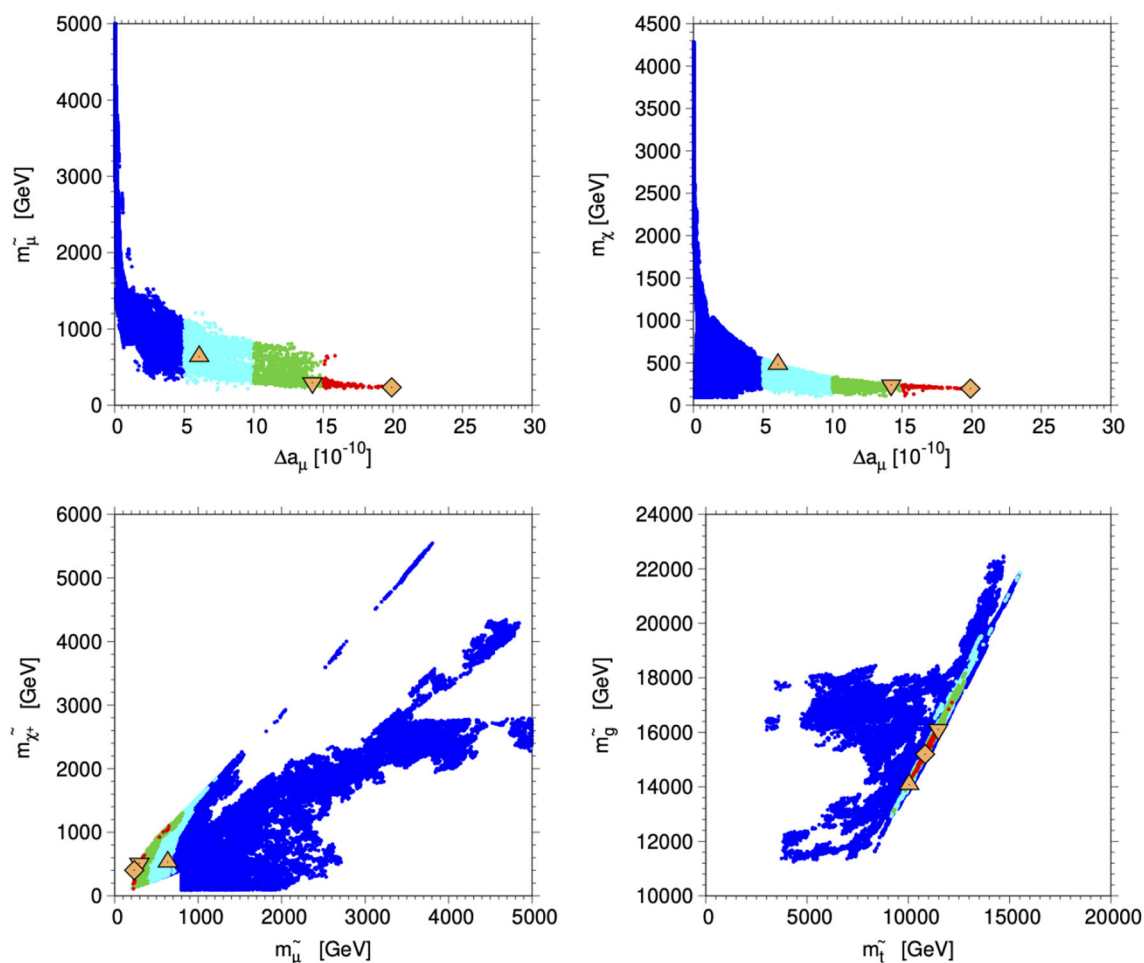


**Fig. 8** As in Fig. 6, displaying the allowed values of sparticle masses in the NUGM as functions of  $\Delta a_\mu$ . Only the upper limit on the cosmological range  $\Omega_\chi h^2 \leq 0.1236$  is imposed

the cold dark matter density is interpreted as an upper limit on the LSP density) and the right panels (where the LSP is assumed to dominate the Planck density range) is that in the latter case there is limited overlap between the ranges of  $m_\chi$  where the Bino and Wino components may dominate.

For models in which the Bino is the LSP, its relic density is determined by various annihilation and coannihilation channels. For relatively low Bino masses, annihilations in what was termed the bulk region of the the MSSM parameter space together with Bino-stau coannihilations dominate [58]. In the CMSSM, these have long been excluded (at the time, by the LEP lower bound on the Higgs mass), but this is not an issue in the NUGM. At larger masses, Bino-Wino and Bino-chargino coannihilations [145–149] become important. When the LSP is predominantly a Wino, it is interesting to note that when the Sommerfeld enhancement [150] of Wino annihilations is included, typically a narrow range of Wino masses with  $m_{\tilde{W}} \simeq 3$  TeV is required to attain  $\Omega_{\tilde{W}} h^2 = 0.12$  [151–155]. This accounts for the large-mass end of the horizontal strip seen in the lower panels of Fig. 4. The Wino

relic density is typically smaller for lower masses, accounting for the elongated strip in the lower left panel. In the lower right panel the strip extends down to roughly 2 TeV, where nominally the relic density would be relatively low. However for these points, the relic density is controlled by Wino-Bino coannihilation, as the Bino is nearly degenerate with the Wino and both states contribute to the relic density, which is actually enhanced.

For completeness, we display in Fig. 5 the magnitudes of the Higgsino components in our NUGM sample. We see that these components are generally small, in the range  $10^{-2}$ – $10^{-3}$ , and do not exhibit much dependence on either  $m_\chi$  or  $\Delta a_\mu$ . Results for the full sample are shown in the left panels, and for models with  $\Omega_\chi h^2$  within the range of cold dark matter density favored by Planck in the right panels.

The upper left panel of Fig. 6 displays our results for the relic density from the scan of parameters in the NUGM. These points are color-coded according to their values of  $\Delta a_\mu$ . We also show in orange a comparison sample of CMSSM points, for which  $M_1 = M_2 = M_3$ . We see that

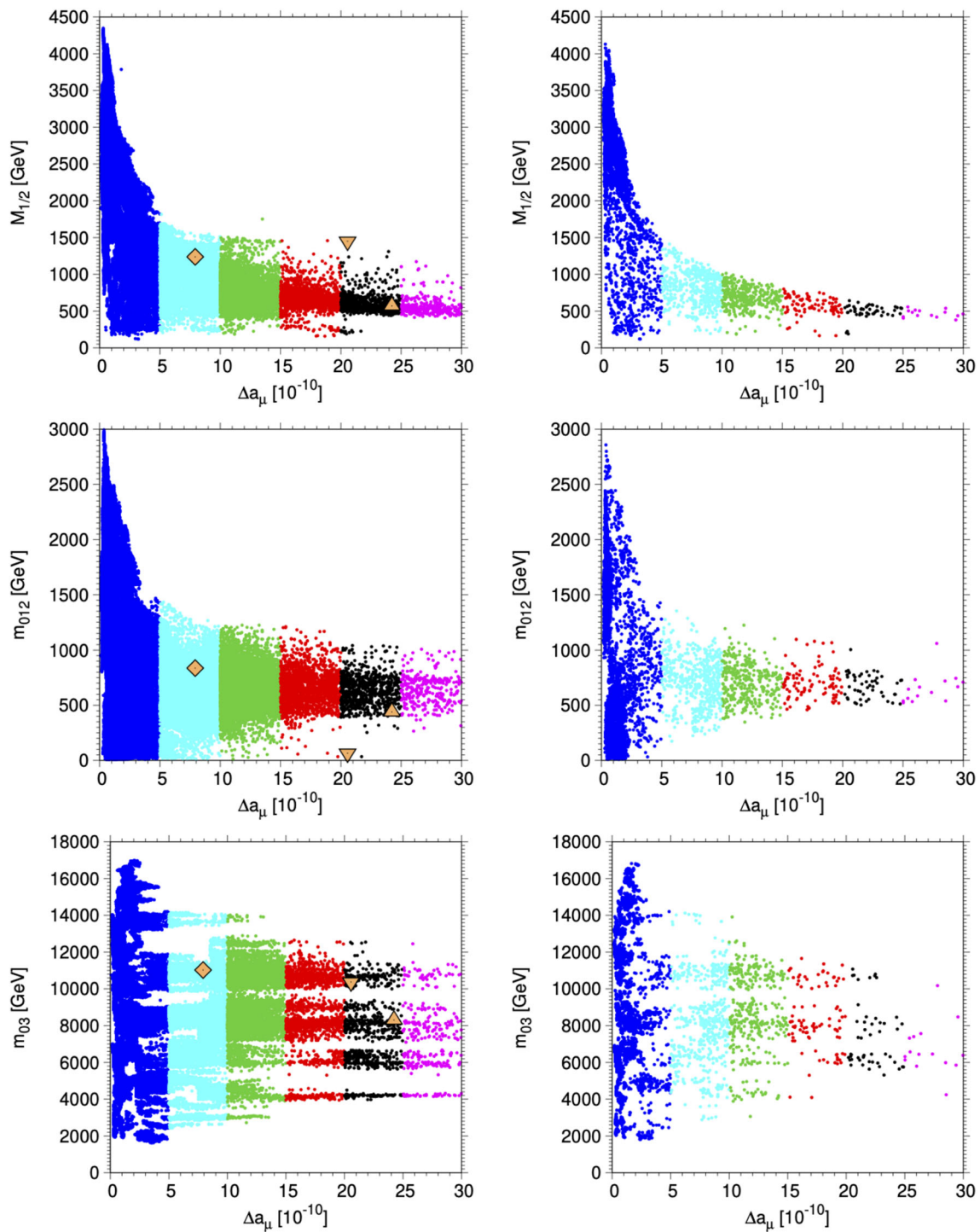


**Fig. 9** The allowed values of  $M_{1/2}$ ,  $m_{012}$  and  $m_{03}$  in the NUHM3 model as functions of  $\Delta a_\mu$ , for points with  $\Omega_\chi h^2 \leq 0.1236$  on the left and points with  $0.1164 \leq \Omega_\chi h^2 \leq 0.1236$  on the right. The triangles in the left planes indicate the locations of the NUHM3 benchmark points discussed in Sect. 5 below

these yield only very small values of  $\Delta a_\mu$ , as expected. We note also in the upper panels of Fig. 6 that the NUGM points yield only  $\Delta a_\mu \lesssim 20 \times 10^{-10}$ . The reason for this is apparent in the upper right panel which shows the value of  $m_H$  as a function of  $\Delta a_\mu$ : larger values of  $\Delta a_\mu$  correspond to  $m_H$

outside the specified range. We see in the upper left panel of Fig. 6 that most of the allowed points yield values of  $\Omega_\chi h^2$  below the range specified above. Those points whose relic density are restricted to the range  $0.1164 \leq \Omega_\chi h^2 \leq 0.1236$  are shown in Fig. 7. This restriction is immediately apparent

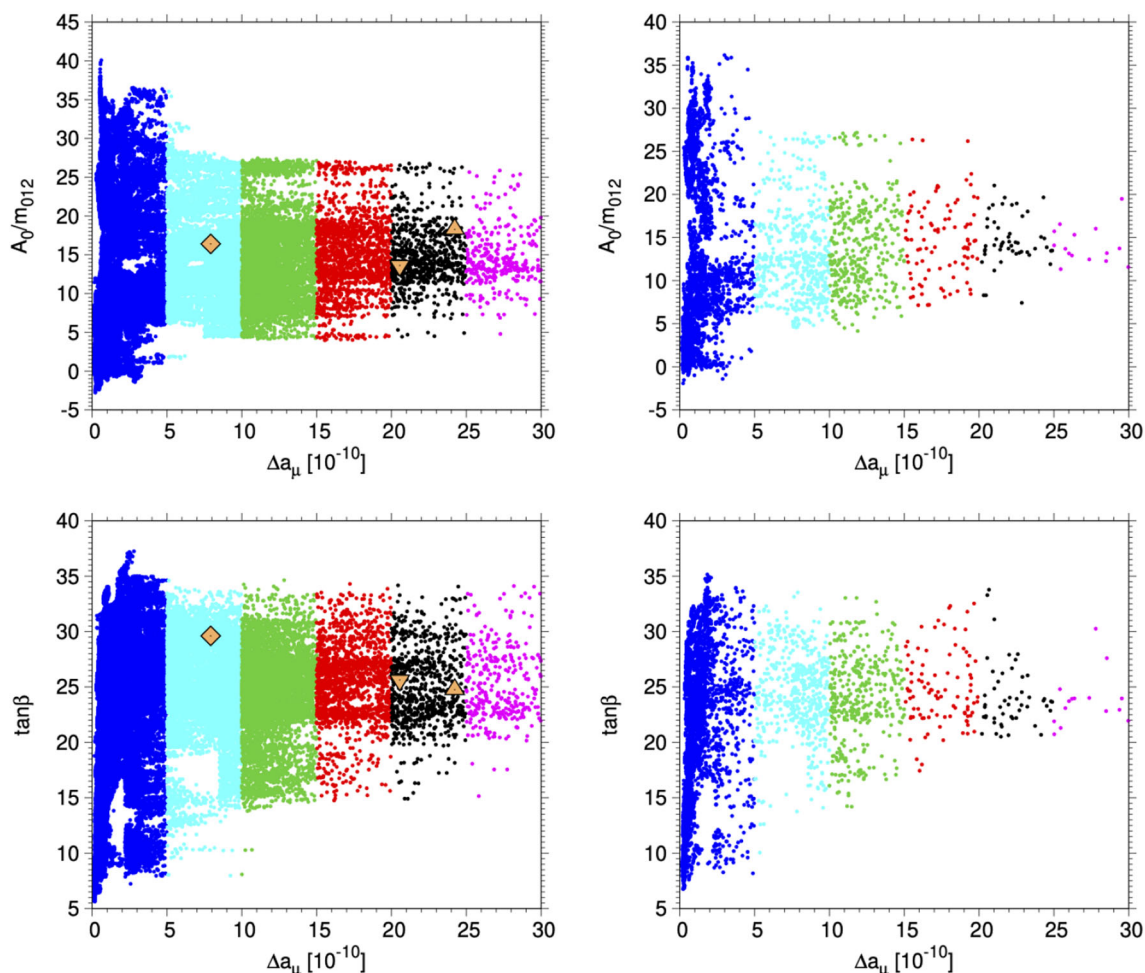


**Fig. 10** As in Fig. 9, displaying the allowed values of  $A_0/m_{012}$  and  $\tan\beta$  in the NUHM3 model as functions of  $\Delta a_\mu$ , for points with  $\Omega_\chi h^2 \leq 0.1236$  on the left and points with  $0.1164 \leq \Omega_\chi h^2 \leq 0.1236$  on the right

in the upper left panel of Fig. 7, but has little impact in the  $(\Delta a_\mu, m_H)$  plane shown in the upper right panel.

The lower panels of Figs. 6 and 7 show scatter plots of the LSP mass,  $m_\chi$ , vs the spin-independent (SI) LSP-proton scattering cross section (left) and the spin-dependent (SD) LSP-proton scattering cross section (right). In Fig. 6 the scattering cross sections have been scaled by a factor  $\Omega_\chi h^2/0.12$  to compensate for the reduced value of  $\Omega_\chi h^2$ , but no such scaling is done in Fig. 7. We see in all of these panels that the NUGM cross sections are orders of magnitude below the current experimental upper limits, below the estimated level of the neutrino ‘fog layer’ [156] except for some points with  $\Delta a_\mu < 5 \times 10^{-10}$ , whereas the CMSSM can yield values of the SI LSP-proton scattering cross section above the corresponding experimental limit, and values of the SD LSP-proton scattering cross section that are only slightly below the experimental limit. Note that we do not show the neutrino fog line in the spin-dependent case as it is highly dependent on the detector material used [156].

Figure 8 displays predictions for some sparticle masses in the NUGM, using the same color coding as in Fig. 2. We see in the upper left panel how the range of smuon masses is correlated with the value of  $\Delta a_\mu$ , and in the upper right panel we see similar behavior for the LSP mass,  $m_\chi$ . As expected the lower smuon and LSP masses are correlated with larger values of  $\Delta a_\mu$ . The correlation between the masses of the smuon and the lighter (Wino-like) chargino,  $\chi^\pm$ , is shown in the lower left panel of Fig. 8, and the correlation between the stop and gluino masses is shown in the lower right panel.<sup>4</sup> We note that large values of  $\Delta a_\mu$  correspond to large values of these masses, well beyond the reach of LHC experiments. In the NUGM, while the smuon mass is restricted to  $\lesssim 200$  GeV if  $\Delta a_\mu > 15 \times 10^{-10}$ , we find that  $m_{\tilde{\tau}} > 11$  TeV and  $m_{\tilde{g}} \sim 15$  TeV, far beyond the reach of the LHC. These

<sup>4</sup> Points in this figure are only subject to the upper limit on the relic density. Restricting to the narrow range of relic densities would only thin the density of points shown, but has little impact on the correlations of  $m_{\tilde{\mu}}$  and  $m_\chi$  with  $\Delta a_\mu$ .

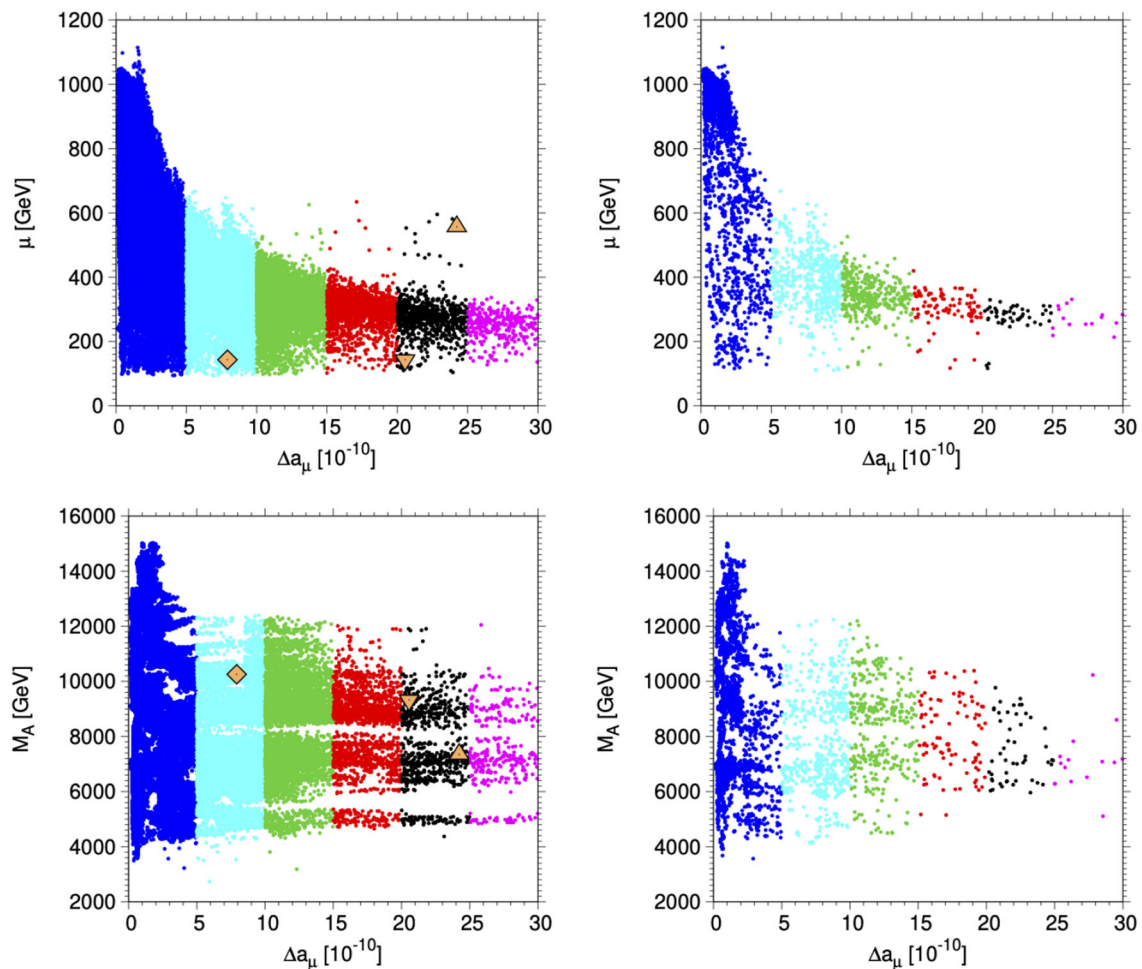


**Fig. 11** As in Fig. 9, displaying the allowed values of  $\mu$  and  $M_A$  in the NUHM3 model as functions of  $\Delta a_\mu$ , for points with  $\Omega_\chi h^2 \leq 0.1236$  on the left and points with  $0.1164 \leq \Omega_\chi h^2 \leq 0.1236$  on the right

results illustrate how the NUGM can reconcile a relatively large value of  $\Delta a_\mu$  with the favored range of  $\Omega_\chi h^2$  and the theoretical calculation of  $m_H$ . This reconciliation requires, in addition, that  $\mu \sim 8$  TeV.

#### 4.2 Non-universal Higgs and third-generation scalar mass model (NUHM3)

Our analysis of the model with non-universal Higgs and third-generation scalars (NUHM3) proceeds along similar lines to the case of the NUGM analysis above. In the NUHM3 case the scan ranges for the seven model parameters are<sup>5</sup>

$$M_{1/2} = 0 - 6 \text{ TeV},$$

$$m_{012} = 0 - 6 \text{ TeV},$$

<sup>5</sup> As noted earlier, the choice of  $\mu$  and  $M_A$  is equivalent to using the soft supersymmetry-breaking masses  $m_{H_1}$  and  $m_{H_2}$ . Using the former allows a more efficient search of parameters sets making a sizeable contribution to  $\Delta a_\mu$ .

$$m_{03} = 0 - 20 \text{ TeV},$$

$$\mu = 0 - 5 \text{ TeV},$$

$$M_A = 0 - 20 \text{ TeV},$$

$$|A_0/m_0| = 0 - 40,$$

$$\tan \beta = 1 - 50. \tag{6}$$

As in the NUGM case, the supersymmetry-breaking mass parameters are input at the GUT scale and run down to the electroweak scale. Inputs that do not yield a neutralino LSP, lead to a tachyonic Higgs pseudoscalar, or do not satisfy the electroweak symmetry-breaking minimization conditions are discarded.

In our scan of the seven-dimensional parameter space of the NUHM3, the MCMC chains provide us with 600,000 points initially. Some 100,000 of them pass the kinematical constraints and have a neutralino LSP. Of these, about 60,000 points satisfy the conditions  $m_H = 125 \pm 2$  GeV and  $\Omega_\chi h^2 \leq 0.1236$ , and about 5,000 points satisfy the stricter condition  $0.1164 \leq \Omega_\chi h^2 \leq 0.1236$ .

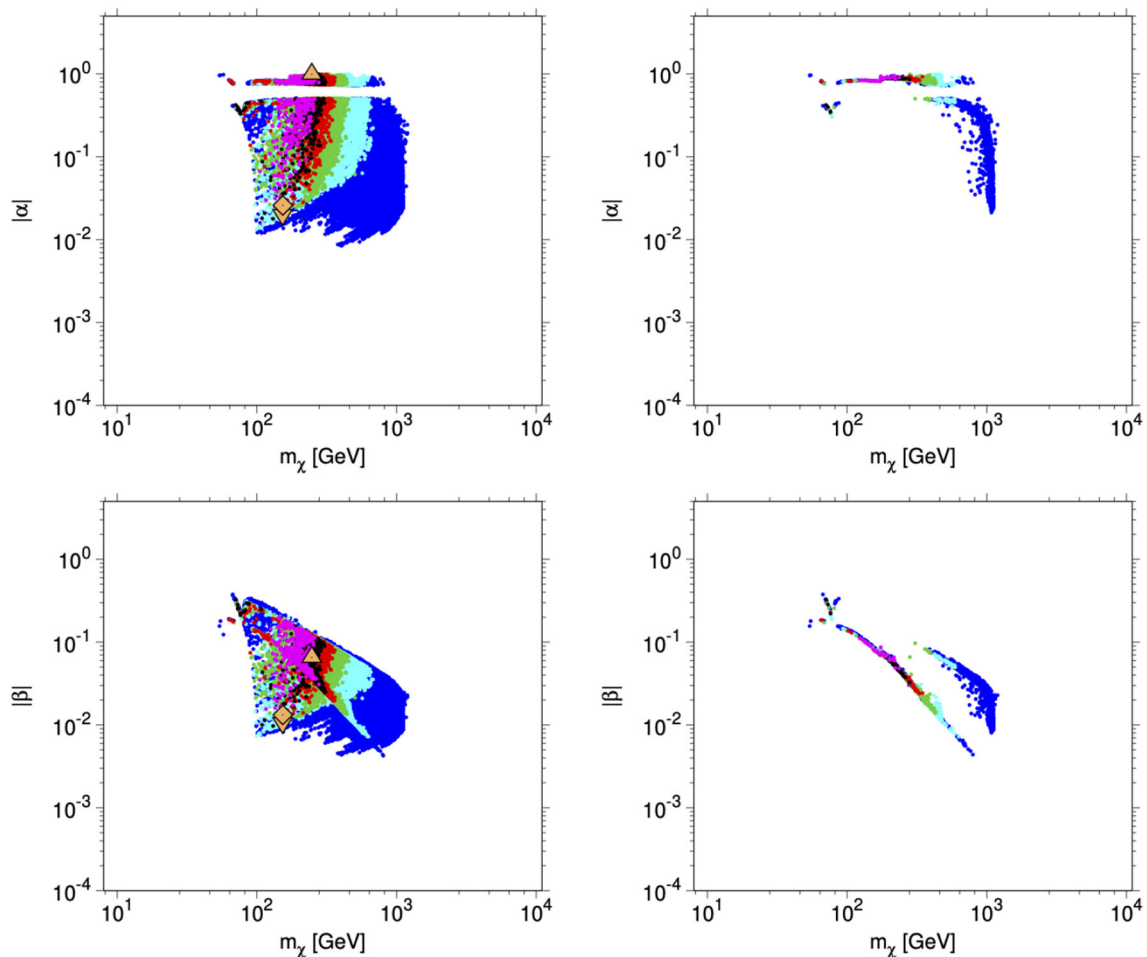


**Fig. 12** The Bino (upper panels) and Wino (lower panels) components  $\alpha$  and  $\beta$ , respectively, of the LSP for the NUHM3 points shown in Fig. 9 as functions of  $m_\chi$ . The color coding corresponds to the values of  $\Delta a_\mu$  shown in Fig. 9

We show in Figs. 9, 10, and 11 the values of the NUHM3 input parameters for points that survive all of the constraints discussed above. As for the NUGM, these are color-coded in intervals of  $\Delta a_\mu = 5 \times 10^{-10}$ . We see that values of  $\Delta a_\mu$  as large as  $30 \times 10^{-10}$  are possible, but for relatively few points when the LSP density is restricted to the Planck determination of  $\Omega_\chi h^2$  (right panels). The parameter sets yielding large values of  $\Delta a_\mu$  tend to prefer relatively small values of the common gaugino mass  $M_{1/2}$ . As we see from the top right panel of Fig. 9,  $M_{1/2} \simeq 500$  GeV when the LSP makes up all of the dark matter. Similarly, when  $\Delta a_\mu$  is large the common first- and second-generation scalar mass  $m_{012}$  also takes low values with  $m_{012} \simeq 500\text{--}700$  GeV preferred. In contrast, the spread third-generation scalar mass  $m_{03}$  is generally much larger, so as to accommodate a large stop mass as needed to provide an acceptable value of  $m_H$ . While the data appear to select somewhat distinct values of  $m_{03}$  at large  $\Delta a_\mu$  in the bottom left panel of Fig. 9, this is due to limitations of the MC sampling, and does not affect the overall envelope of allowed points in the  $(\Delta a_\mu, m_{03})$  plane.

The triangles in the left planes indicate the locations of the NUHM3 benchmark points discussed in Sect. 5 below: none of the NUHM3 benchmarks saturate the Planck cold dark matter density.

Figure 10 indicates that the NUHM3 models are relatively insensitive to  $A_0$  and  $\tan \beta$ . There is a wide range of values of  $A_0/m_{012}$  that yield large values of  $\Delta a_\mu$ , though the number of points found is greatly diminished when we restrict the density to the cosmological range as we see when comparing the left and right panels. We note that although the values of  $A_0/m_{012}$  are large, namely  $\mathcal{O}(20)$ ,  $A_0/m_{03}$  is only  $\mathcal{O}(1)$ . Compared to the NUGM discussed in the previous section, values of  $\tan \beta$  found here are relatively high, of order 25.

In contrast to  $A_0/m_{012}$ , the value of  $\mu$  shown in Fig. 11 does correlate with  $\Delta a_\mu$ , with lower values of  $\mu$  preferred for large  $\Delta a_\mu$ . When the LSP density is restricted to the cosmological range,  $\mu \lesssim 300$  GeV is preferred as seen in the upper right panel of Fig. 11. On the hand, a large range of values of  $M_A$  between 5 and 10 TeV are found at large when  $\Delta a_\mu$  is large and the LSP density is not restricted. With the

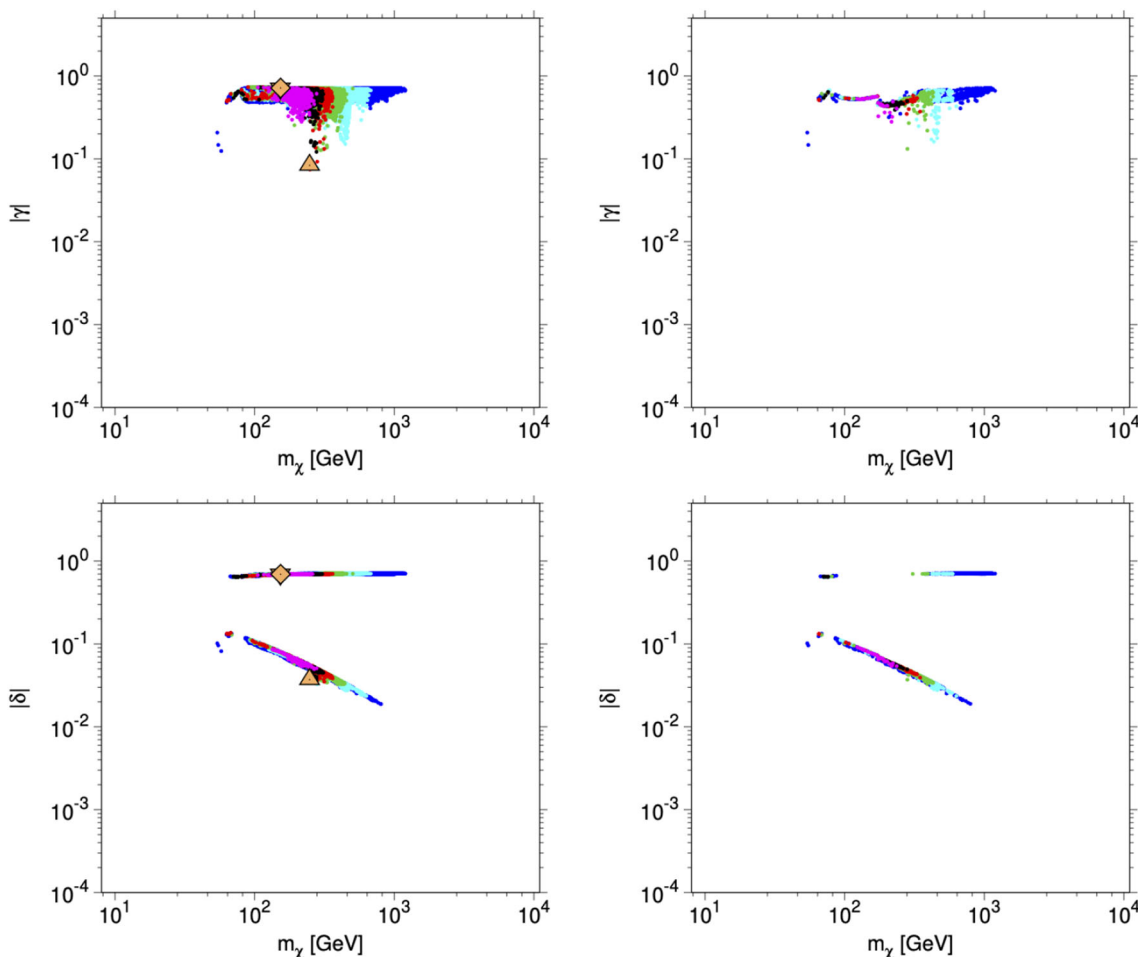


**Fig. 13** The Higgsino components  $\gamma$  and  $\delta$ , respectively, of the LSP for the NUHM3 points shown in Fig. 9 as functions of  $m_\chi$ . The color coding corresponds to the values of  $\Delta a_\mu$  shown in Fig. 9. Though difficult to see, benchmark points B and C are sitting on top of each other in this figure

relic density restricted, there are again fewer points at large  $\Delta a_\mu$ .

We display in Fig. 12 the composition of the LSP in these NUHM3 points. The left panels display points with  $\Omega_\chi h^2 \leq 0.1236$  and the right panel shows points with  $0.1164 \leq \Omega_\chi h^2 \leq 0.1236$ . In both cases  $m_H = 125 \pm 2$  GeV. Unlike the case of the the NUGM, the Bino component  $\alpha$  may or may not dominate. Indeed, we find two distinct populations, those with  $|\alpha| \sim 1$  and those with much lower values, for which one of the Higgsino components dominates. The two Higgsino components,  $\gamma$  and  $\delta$  are displayed in Fig. 13, again for points with  $\Omega_\chi h^2 \leq 0.1236$  in the left panels and for points with  $0.1164 \leq \Omega_\chi h^2 \leq 0.1236$  in the right panels, and  $m_H = 125 \pm 2$  GeV. The Wino component  $\beta$  is mostly in the range  $[0.1, 0.01]$  though values as large as  $\sim 0.3$  are attained for a few points.

Figure 14 displays some two-dimensional projections of the NUHM3 points allowed when the relic LSP density is constrained only by the upper limit  $\Omega_\chi h^2 \leq 0.1236$ . Here, in addition to the color coding for different  $5 \times 10^{-10}$  ranges

of  $\Delta a_\mu$ , we have colored orange points in a sample with  $m_{012}=m_{03}$  (the NUHM2). As already commented, there are NUHM3 points compatible with  $m_H = 125 \pm 2$  GeV that have  $\Delta a_\mu$  as large as  $30 \times 10^{-10}$ , whereas the NUHM2 points all have very small  $\Delta a_\mu$ , as was the case for the CMSSM sample mentioned in connection with our NUGM analysis above. The scattering cross sections are shown in the lower panels of Fig. 14. In this case, as in the NUGM, we plot the scattering cross section scaled by the density  $\Omega_\chi h^2/0.12$ , so as to correspond better to the scattering rate in a detector. There is wide range of the SI and SD cross sections that are allowed by experiment for points with a low density. Measurements of the SI cross section exclude most of the NUHM3 sample, but some points with  $\Delta a_\mu \lesssim 15 \times 10^{-10}$  are allowed, along with many of the NUHM2 points. The present experimental limit of the SD cross section is a weaker constraint on the NUHM3 sample, and all the NUHM2 sample predicts values well below the experimental limit.

Figure 15 shows an analogous set of NUHM3 parameter planes where the LSP density is restricted to the Planck

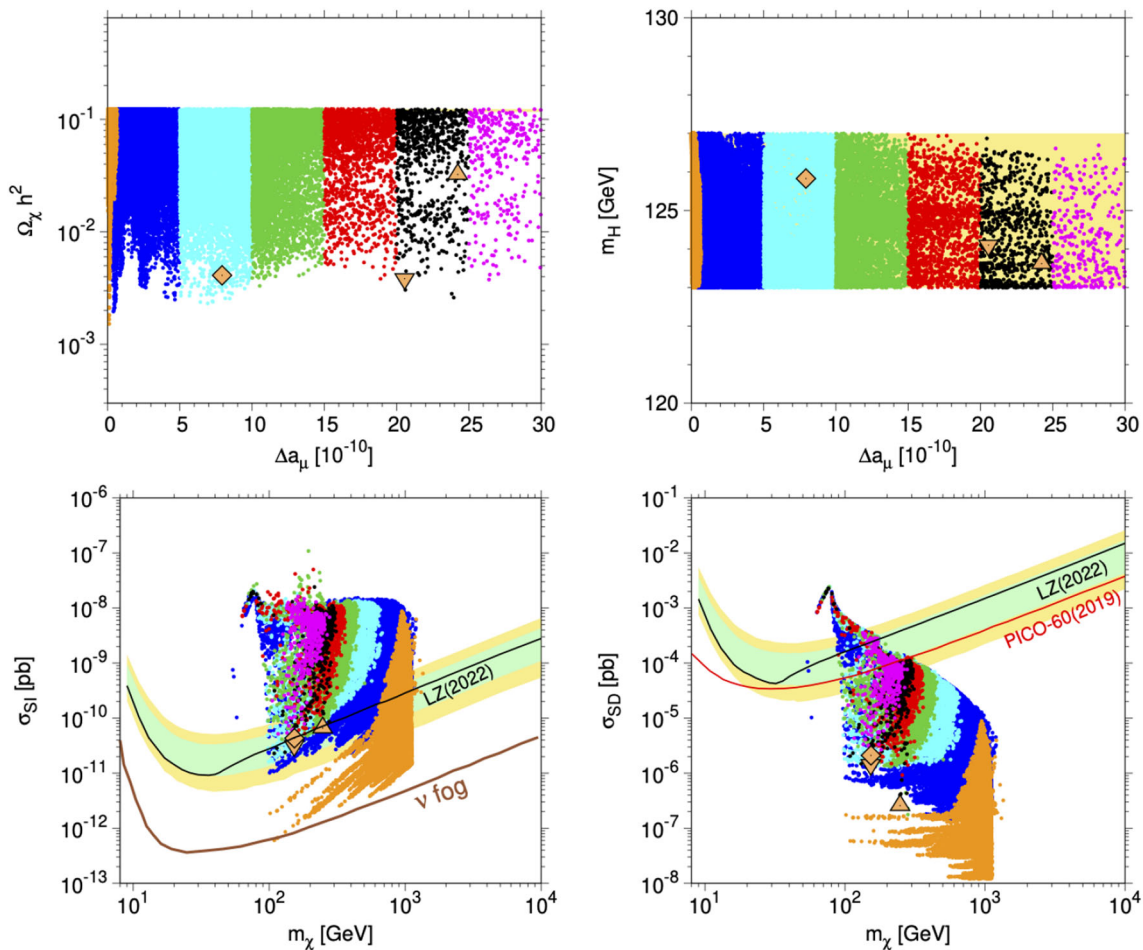


**Fig. 14** As in Fig. 6, but for the NUHM3 model, allowing  $M_{1/2}, m_{012}, m_{03}, \mu, M_A, A_0$  and  $\tan \beta$  to vary, showing all points with  $\Omega_\chi h^2 \leq 0.1236$  and rescaling the direct detection cross sections by a factor  $\Omega_\chi h^2/0.12$ . The orange points correspond to a sample with  $m_{012}=m_{03}$ , i.e., the NUHM2 model

range  $0.1164 \leq \Omega_\chi h^2 \leq 0.1236$ . We see that there are still many such points with  $m_H$  within  $\pm 2$  GeV of the measured Higgs mass. The lower left panel of Fig. 15 shows, however, that the NUHM3 sample points generally have values of the SI cross section that are excluded, with the remainder lying above the neutrino ‘fog layer’ [156], and that some of the NUHM3 sample also predicts values of the SD cross section that are excluded. This is why none of the NUHM3 benchmarks saturate the Planck cold dark matter density. However, some (all) of the NUHM2 sample predicts values of the SI (SD) cross section that are compatible with experiment.

Figure 16 displays the allowed ranges of  $m_{\tilde{\mu}}$  and  $m_\chi$  as functions of  $\Delta a_\mu$  in the upper panels, and the  $(m_{\tilde{\mu}}, m_{\chi^\pm})$  and  $(m_{\tilde{\tau}}, m_g)$  correlations in the lower panels, all for the sample with  $\Omega_\chi h^2 \leq 0.1236$ . We see that points with  $\Delta a_\mu > 20 \times 10^{-10}$  have  $m_{\tilde{\mu}}$  and  $m_\chi \lesssim 300$  GeV, whereas larger masses are allowed for models with smaller  $\Delta a_\mu$ . The  $(m_{\tilde{\mu}}, m_\chi)$  correlation is tighter for points with  $\Delta a_\mu > 5 \times 10^{-10}$ , but the larger values of  $m_{\tilde{\mu}}$  and  $m_\chi$  allowed for smaller  $\Delta a_\mu$  are

largely uncorrelated. We also note that  $m_{\tilde{g}}$  can be large when  $\Delta a_\mu > 5 \times 10^{-10}$ , but is restricted to  $m_{\tilde{g}} \lesssim 3$  TeV for larger  $\Delta a_\mu$ . Qualitatively similar features remain when we impose  $0.1164 \leq \Omega_\chi h^2 \leq 0.1236$ , albeit with a smaller sample.

As commented above, the LHC constraints on squark and gluino masses in simplified models such as the CMSSM are weakened in more general models where several different mass parameters and decay modes must be taken into account when deriving mass limits. We are unaware of any dedicated studies of the NUHM3 but note, for example, that a detailed study of the pMSSM using  $\sim 36/\text{fb}$  LHC Run 2 data found that squarks and gluinos could have masses as low as  $\sim 700\text{--}800$  GeV: see the right panels of Fig. 2 of [38]. Limits at these levels would impinge on a small corner of the lower right panel of Fig. 16 but not exclude the vast majority of NUHM3 points displayed. It would be desirable to update this analysis to include all available LHC Run 2 data, and extend it to the NUHM3, but that is beyond the scope of this paper. Such analyses would exclude larger ranges of gluino and

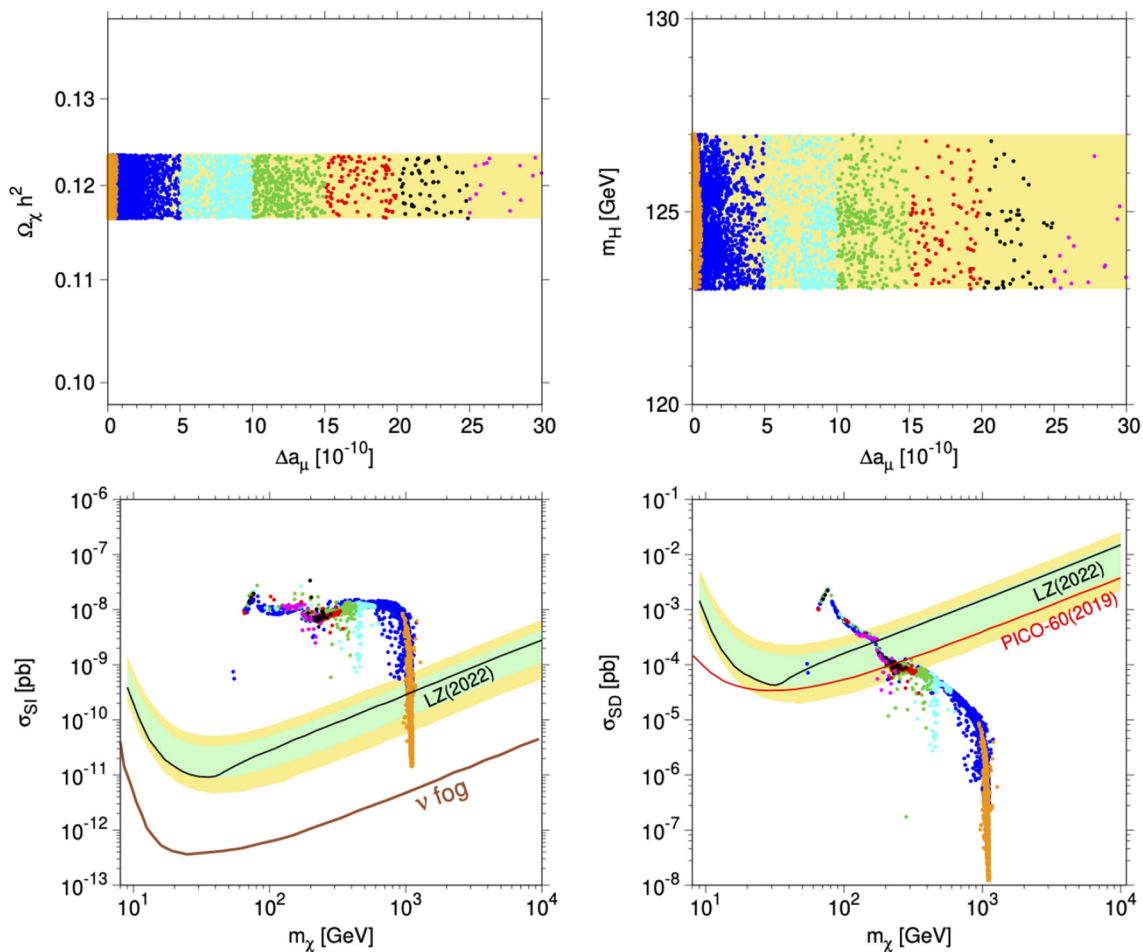


**Fig. 15** As in Fig. 14, but restricting the LSP density to the Planck range  $0.1164 \leq \Omega_\chi h^2 \leq 0.1236$

squark masses but we do not expect our overall conclusions to change.

### 5 Benchmark scenarios

Based on the analysis in Sect. 4.1, we have selected three benchmark NUGM models, labeled A, B, and C. The sets of input parameters for these benchmarks is given in Table 1. They are distinguished primarily by the value of  $\Delta a_\mu$ . The calculated relic density, value of  $\Delta a_\mu$ , and the spin-independent and -dependent scattering cross sections as well as some representative masses are provided in Table 2. Each of these points was chosen to yield a relic density close to the Planck value of the cold dark matter density.

As seen in Fig. 1, the contributions to the anomalous muon magnetic moment for these points cover the range of  $\Delta a_\mu \lesssim 20 \times 10^{-10}$ , i.e., within  $1\sigma$  of the value of  $\Delta a_\mu$  indicated by the data-driven theoretical estimate [4] and covering the ranges favored by lattice calculations [7, 8], as well as the CMD-3 estimate [9] and the recent phenomenologi-

cal analysis in [10]. The NUGM can provide values of  $\Delta a_\mu$  significantly larger than those found in the CMSSM, constituting a major improvement over the CMSSM.

As noted earlier, models with relatively large  $\Delta a_\mu$  tend to have relatively low elastic scattering cross sections. The values for  $\sigma_{SI}$  and  $\sigma_{SD}$  for the three benchmark points are also given in Table 2. All three of these benchmark points have a Bino-like LSP whose relic density is determined primarily by stau coannihilation [87–95]. The masses of the LSP, lighter chargino (Wino-like), left-handed smuon, lighter stau, gluino and lighter stop are also given in the Table. Their spectra are somewhat similar and have relatively low masses for the color-neutral states, which may be within reach of the LHC. However, the stop and gluino have in each case masses in excess of 10 TeV, beyond the reach of the LHC. The benchmarks are presented in Table 2 and indicated by yellow symbols ( $\Delta$ ,  $\nabla$  and  $\diamond$ ) in the figures.

We have also selected a set of three benchmark points for the NUHM3. In this case, even though there are many points for which the relic density is of order 0.12, these points are excluded since their spin-independent cross sections are

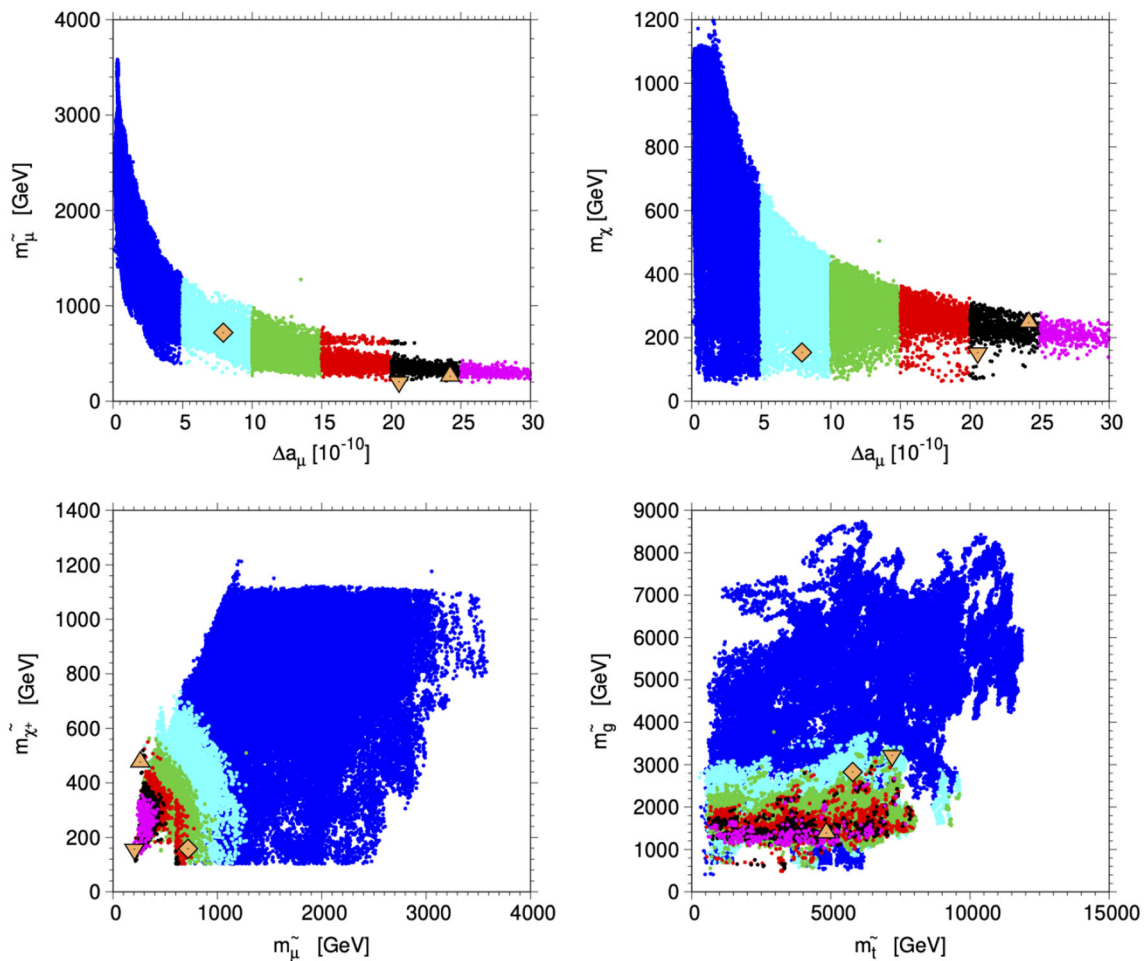


**Fig. 16** As in Fig. 8, but displaying the allowed ranges of sparticle masses in the NUHM3 model as functions of  $\Delta a_\mu$

**Table 1** Benchmark points for the NUGM

	$M_1$	$M_2$	$M_3$	$m_0$	$A_0/m_0$	$\tan \beta$
A ( $\Delta$ )	1218	799	7245	676	0.4	17
B ( $\nabla$ )	730	828	8365	541	-0.6	7
C ( $\diamond$ )	626	695	7852	550	0.0	7

too large, even when theoretical uncertainties are taken into account [141]. We use Fig. 14 to select benchmark points that have a broad range of contributions to  $\Delta a_\mu \lesssim 24 \times 10^{-10}$  but do not violate any of the constraints considered. However, as discussed earlier, none of them saturate the Planck cold dark matter density. The benchmarks are presented in Table 3 and indicated by yellow symbols ( $\Delta$ ,  $\nabla$  and  $\diamond$ ) in the figures. As in the case of the NUGM, we note that the masses of the color-neutral sparticles at these benchmarks are light enough to be potentially detectable at the LHC. Again as in the NUGM case, however, the colored sparticles are generally too heavy to be found at the LHC. An exception is the

**Table 2** Observables and masses for the NUGM benchmark points in Table 1. The LSP is Bino-like for these points

	A ( $\Delta$ )	B ( $\nabla$ )	C ( $\diamond$ )
$\Omega_\chi h^2$	0.118	0.123	0.118
$\Delta a_\mu (10^{-10})$	6.1	14.2	19.9
$\sigma_{SI} (10^{-13} pb)$	1.0	2.2	2.1
$\sigma_{SD} (10^{-11} pb)$	2.6	1.2	1.5
$m_\chi$	480	240	196
$m_{\chi_1^+}$	529	513	402
$m_{\tilde{\mu}_{L,R}}$	637	296	234
$m_{\tilde{\tau}_1}$	513	258	214
$m_{\tilde{g}}$	14,080	16,110	15,200
$m_{\tilde{t}_1}$	10,040	11,480	10,830

gluino at benchmark point A, which is lighter than the lower limit set in simplified models such as the CMSSM. However, as seen in the bottom panels of Fig. 2 in [38], this limit may be relaxed in more general models, and the light gluino of

**Table 3** Benchmark points for the NUHM3 model

	$M_{1/2}$	$m_{012}$	$m_{03}$	$\mu$	$M_A$	$A_0/m_{012}$	$\tan \beta$
A ( $\Delta$ )	571	440	8305	557	7340	18.3	25
B ( $\nabla$ )	1450	65	10,374	143	9317	13.6	26
C ( $\diamond$ )	1238	837	11,025	143	10,239	16.4	30

**Table 4** Observables and masses for the NUHM3 benchmark points in Table 3. At point A the LSP is a Bino, while at points B and C it is a Higgsino. The re-scaled direct detection cross sections ( $\sigma \times \Omega_\chi h^2/0.12$ ) for these points are smaller than the LZ bound, so these points lie below the black curve in Fig. 14

	A ( $\Delta$ )	B ( $\nabla$ )	C ( $\diamond$ )
$\Omega_\chi h^2$	$3.24 \times 10^{-2}$	$3.84 \times 10^{-3}$	$4.11 \times 10^{-3}$
$\Delta a_\mu (10^{-10})$	24.2	20.6	7.9
$\sigma_{SI} (pb)$	$2.5 \times 10^{-10}$	$1.0 \times 10^{-9}$	$1.2 \times 10^{-9}$
$\sigma_{SI} (pb)$ re-scaled	$6.6 \times 10^{-11}$	$3.2 \times 10^{-11}$	$4.2 \times 10^{-11}$
$\sigma_{SD} (pb)$	$9.5 \times 10^{-7}$	$4.5 \times 10^{-5}$	$6.2 \times 10^{-5}$
$\sigma_{SD} (pb)$ re-scaled	$2.6 \times 10^{-7}$	$1.4 \times 10^{-6}$	$2.1 \times 10^{-6}$
$m_\chi$	247	153	153
$m_{\chi_1^+}$	476	157	158
$m_{\tilde{\mu}_{L,R}}$	261	205	719
$m_{\tilde{t}_1}$	7759	9869	9791
$m_{\tilde{g}}$	1388	3219	2829
$m_{\tilde{t}_1}$	4837	7202	5785

point A may still be allowed and offer prospects for future detection at the LHC, a point requiring further study (Table 4).

### 6 Summary

We have shown in this paper that a significant supersymmetric contribution to the muon anomalous magnetic moment is possible if one relaxes the restrictive unification conditions on the gaugino and sfermion masses made in specific models such as the CMSSM and the NUHM2. In particular, in a model with non-unified gaugino masses one can find  $\Delta a_\mu \sim 17 \times 10^{-10}$ , e.g., if  $M_{1,2} \sim 600$  GeV and  $M_3 \sim 8$  TeV. In the case of non-universal Higgs and third-generation sfermion masses, one can find even larger  $\Delta a_\mu \lesssim 24 \times 10^{-10}$  for first- and second-generation sfermion masses  $\sim 400$  GeV and third-generation sfermion masses  $\sim 8$  TeV. These possibilities are illustrated by the benchmark points whose predictions for  $\Delta a_\mu$  are shown in Fig. 1.

These benchmark scenarios predict, in general, relatively light color-neutral sparticles that may be detectable at the LHC. Figure 17 shows the locations of the NUGM and NUHM3 benchmark points in the  $(m_{\tilde{\mu}}, m_\chi)$  plane. We see

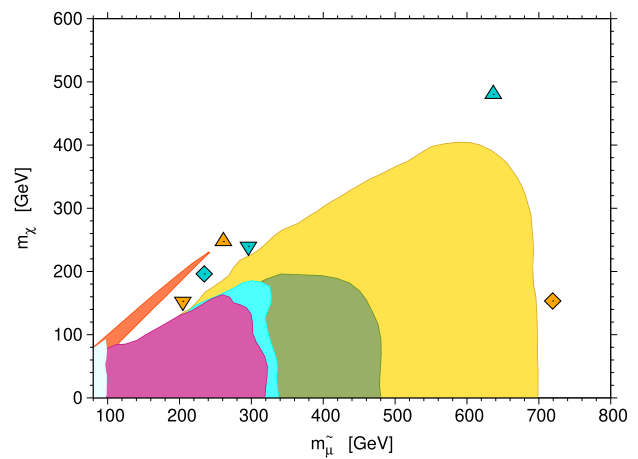


**Fig. 17** The benchmark points for NUGM (cyan symbols) and NUHM3 (orange symbols), where triangle is point A, inverted triangle B and diamond C. The shaded regions are excluded by ATLAS dilepton searches at the LHC, see [138, 140]; the colors correspond to different searches, as explained in [139]

that they are allowed by the current ATLAS constraints [23], but likely to be vulnerable to foreseeable improvements in the LHC search sensitivity. On the other hand, the strongly-interacting sparticles must be heavier than the color-neutral sparticles, in particular so as to yield a Higgs mass in the experimental range. A consequence of this requirement is that the rates for direct detection of scattering on nuclei are typically small in the NUGM, lost in the ‘neutrino fog’ except for some points with  $\Delta a_\mu < 5 \times 10^{-10}$ . However, the NUHM3 benchmark points have scattering rates that may be detectable after rescaling.

We have shown in this paper how supersymmetric models could accommodate a discrepancy  $\Delta a_\mu$  between Standard Model prediction and the experimental measurements, whichever of the current theoretical estimates [4, 7, 9, 10] turns out to be more accurate. In all the benchmark scenarios studies, there are prospects for detecting color-singlet sparticles at the LHC, and it is also possible that the gluino might be within experimental reach. Many obituaries for supersymmetry have been pronounced, but in the immortal words of Monty Python [157], it is “not dead yet”, and the anomalous magnetic moment of the muon may yet revive interest in supersymmetry.

**Acknowledgements** The work of J.E. was supported in part by the United Kingdom STFC Grant ST/T000759/1. The work of K.A.O. was supported in part by DOE grant DE-SC0011842 at the University of Minnesota. V.C.S. is grateful to the William I. Fine Theoretical Physics Institute at the University of Minnesota for their financial support and the warm hospitality extended to him during his sabbatical leave. He also acknowledges support from the Simons Foundation Targeted Grant 920184 to the William I. Fine Theoretical Physics Institute.

**Funding** There is no further funding information for this article.

**Data Availability Statement** My manuscript has no associated data. [Author's comment: Data sharing not applicable to this article as no datasets were generated or analysed during the current study.]

**Code Availability Statement** My manuscript has no associated code/software. [Author's comment: Code/Software sharing not applicable to this article as no code/software was generated or analysed during the current study.]

**Open Access** This article is licensed under a Creative Commons Attribution 4.0 International License, which permits use, sharing, adaptation, distribution and reproduction in any medium or format, as long as you give appropriate credit to the original author(s) and the source, provide a link to the Creative Commons licence, and indicate if changes were made. The images or other third party material in this article are included in the article's Creative Commons licence, unless indicated otherwise in a credit line to the material. If material is not included in the article's Creative Commons licence and your intended use is not permitted by statutory regulation or exceeds the permitted use, you will need to obtain permission directly from the copyright holder. To view a copy of this licence, visit <http://creativecommons.org/licenses/by/4.0/>. Funded by SCOAP<sup>3</sup>.

## References

- H.N. Brown [Muon g-2 Collaboration] et al., Phys. Rev. Lett. **86**, 2227–2231 (2001). [arXiv:hep-ex/0102017](https://arxiv.org/abs/hep-ex/0102017)
- G.W. Bennett [Muon g-2 Collaboration] et al., Phys. Rev. D **73**, 072003 (2006). [arXiv:hep-ex/0602035](https://arxiv.org/abs/hep-ex/0602035)
- B. Abi, [Muon g-2 Collaboration] et al., Phys. Rev. Lett. **126**, 141801 (2021). [arXiv:2104.03281](https://arxiv.org/abs/2104.03281) [hep-ex]
- T. Aoyama et al., Phys. Rep. **887**, 1–166 (2020). [arXiv:2006.04822](https://arxiv.org/abs/2006.04822) [hep-ph]
- D.P. Aguillard, [Muon g-2 Collaboration] et al., Phys. Rev. Lett. **131**(16), 161802 (2023). [arXiv:2308.06230](https://arxiv.org/abs/2308.06230) [hep-ex]
- D.P. Aguillard et al. [Muon g-2], [arXiv:2402.15410](https://arxiv.org/abs/2402.15410) [hep-ex]
- S. Borsanyi [BMW Collaboration] et al., Nature **593**(7857), 51–55 (2021). [arXiv:2002.12347](https://arxiv.org/abs/2002.12347) [hep-lat]
- S. Kuberski, PoS LATTICE2023, 125 (2024). <https://doi.org/10.22323/1.453.0125>. [arXiv:2312.13753](https://arxiv.org/abs/2312.13753) [hep-lat]
- F.V. Ignatov et al. [CMD-3 Collaboration], Phys. Rev. Lett. **132**(23), 231903 (2024). [arXiv:2309.12910](https://arxiv.org/abs/2309.12910) [hep-ex]
- M. Davier, A. Hoecker, A.M. Lutz, B. Malaescu, Z. Zhang, [arXiv:2312.02053](https://arxiv.org/abs/2312.02053) [hep-ph]
- A. Boccaletti, S. Borsanyi, M. Davier, Z. Fodor, F. Frech, A. Gardin, D. Giusti, A.Y. Kotov, L. Lellouch, T. Lippert et al., [arXiv:2407.10913](https://arxiv.org/abs/2407.10913) [hep-lat]
- J.R. Ellis, D.V. Nanopoulos, K.A. Olive, Phys. Lett. B **508**, 65–73 (2001). [arXiv:hep-ph/0102331](https://arxiv.org/abs/hep-ph/0102331)
- L.L. Everett, G.L. Kane, S. Rigolin, L. Wang, Phys. Rev. Lett. **86**, 3484 (2001). [arXiv:hep-ph/0102145](https://arxiv.org/abs/hep-ph/0102145)
- J.L. Feng, K.T. Matchev, Phys. Rev. Lett. **86**, 3480 (2001). [arXiv:hep-ph/0102146](https://arxiv.org/abs/hep-ph/0102146)
- E.A. Baltz, P. Gondolo, Phys. Rev. Lett. **86**, 5004 (2001). [arXiv:hep-ph/0102147](https://arxiv.org/abs/hep-ph/0102147)
- U. Chattopadhyay, P. Nath, Phys. Rev. Lett. **86**, 5854 (2001). [arXiv:hep-ph/0102157](https://arxiv.org/abs/hep-ph/0102157)
- S. Komine, T. Moroi, M. Yamaguchi, Phys. Lett. B **506**, 93 (2001). [arXiv:hep-ph/0102204](https://arxiv.org/abs/hep-ph/0102204)
- J. Hisano, K. Tobe, Phys. Lett. B **510**, 197–204 (2001). [arXiv:hep-ph/0102315](https://arxiv.org/abs/hep-ph/0102315)
- R. Arnowitt, B. Dutta, B. Hu, Y. Santoso, Phys. Lett. B **505**, 177 (2001). [arXiv:hep-ph/0102344](https://arxiv.org/abs/hep-ph/0102344)
- S.P. Martin, J.D. Wells, Phys. Rev. D **64**, 035003 (2001). [arXiv:hep-ph/0103067](https://arxiv.org/abs/hep-ph/0103067)
- H. Baer, C. Balazs, J. Ferrandis, X. Tata, Phys. Rev. D **64**, 035004 (2001). [arXiv:hep-ph/0103280](https://arxiv.org/abs/hep-ph/0103280)
- A.B. Lahanas, D.V. Nanopoulos, V.C. Spanos, Phys. Lett. B **518**, 94–100 (2001). [arXiv:hep-ph/0107151](https://arxiv.org/abs/hep-ph/0107151)
- For a compendium of ATLAS searches for supersymmetry, see <https://twiki.cern.ch/twiki/bin/view/AtlasPublic/SupersymmetryPublicResults>, and for a compendium of CMS searches for supersymmetry see <https://twiki.cern.ch/twiki/bin/view/CMSPublic/PhysicsResultsSUS>
- M. Endo, K. Hamaguchi, S. Iwamoto, T. Kitahara, JHEP **07**, 075 (2021). [arXiv:2104.03217](https://arxiv.org/abs/2104.03217) [hep-ph]
- S. Iwamoto, T.T. Yanagida, N. Yokozaki, Phys. Lett. B **823**, 136768 (2021). [arXiv:2104.03223](https://arxiv.org/abs/2104.03223) [hep-ph]
- Y. Gu, N. Liu, L. Su, D. Wang, Nucl. Phys. B **969**, 115481 (2021). [arXiv:2104.03239](https://arxiv.org/abs/2104.03239) [hep-ph]
- M. Chakraborti, S. Heinemeyer, I. Saha, Eur. Phys. J. C **81**(12), 1114 (2021). [arXiv:2104.03287](https://arxiv.org/abs/2104.03287) [hep-ph]
- P. Cox, C. Han, T.T. Yanagida, Phys. Rev. D **104**(7), 075035 (2021). [arXiv:2104.03290](https://arxiv.org/abs/2104.03290) [hep-ph]
- P. Athron, C. Balázs, D.H. Jacob, W. Kotlarski, D. Stöckinger, H. Stöckinger-Kim, [arXiv:2104.03691](https://arxiv.org/abs/2104.03691) [hep-ph]
- M. Chakraborti, L. Roszkowski, S. Trojanowski, JHEP **05**, 252 (2021). [arXiv:2104.04458](https://arxiv.org/abs/2104.04458) [hep-ph]
- W. Altmannshofer, S.A. Gadam, S. Gori, N. Hamer, JHEP **07**, 118 (2021). [arXiv:2104.08293](https://arxiv.org/abs/2104.08293) [hep-ph]
- Z. Li, G.L. Liu, F. Wang, J.M. Yang, Y. Zhang, JHEP **12**, 219 (2021). [arXiv:2106.04466](https://arxiv.org/abs/2106.04466) [hep-ph]
- J. Ellis, J.L. Evans, N. Nagata, D.V. Nanopoulos, K.A. Olive, Eur. Phys. J. C **81**(12), 1109 (2021). [arXiv:2110.06833](https://arxiv.org/abs/2110.06833) [hep-ph]
- M. Chakraborti, S. Heinemeyer, I. Saha, C. Schappacher, Eur. Phys. J. C **82**(5), 483 (2022). [arXiv:2112.01389](https://arxiv.org/abs/2112.01389) [hep-ph]
- J. Ellis, J.L. Evans, N. Nagata, D.V. Nanopoulos, K.A. Olive, Eur. Phys. J. C **81**(12), 1109 (2021). [arXiv:2110.06833](https://arxiv.org/abs/2110.06833) [hep-ph]
- J. Ellis, J.L. Evans, N. Nagata, D.V. Nanopoulos, K.A. Olive, Eur. Phys. J. C **81**(12), 1079 (2021). [arXiv:2107.03025](https://arxiv.org/abs/2107.03025) [hep-ph]
- F. Wang, L. Wu, Y. Xiao, J.M. Yang, Y. Zhang, Nucl. Phys. B **970**, 115486 (2021). [arXiv:2104.03262](https://arxiv.org/abs/2104.03262) [hep-ph]
- E. Bagnaschi, K. Sakurai, M. Borsato, O. Buchmueller, M. Citron, J.C. Costa, A. De Roeck, M.J. Dolan, J.R. Ellis, H. Flücher et al., Eur. Phys. J. C **78**(3), 256 (2018). [arXiv:1710.11091](https://arxiv.org/abs/1710.11091) [hep-ph]
- F. Wang, K. Wang, J.M. Yang, J. Zhu, JHEP **12**, 041 (2018). [arXiv:1808.10851](https://arxiv.org/abs/1808.10851) [hep-ph]
- A. Aboubrhim, M. Klases, P. Nath, Phys. Rev. D **104**(3), 035039 (2021). [arXiv:2104.03839](https://arxiv.org/abs/2104.03839) [hep-ph]
- H. Baer, V. Barger, H. Serce, Phys. Lett. B **820**, 136480 (2021). [arXiv:2104.07597](https://arxiv.org/abs/2104.07597) [hep-ph]
- J. Ellis, K.A. Olive, V.C. Spanos, I.D. Stamou, Eur. Phys. J. C **83**(3), 246 (2023). [arXiv:2210.16337](https://arxiv.org/abs/2210.16337) [hep-ph]
- G. Aad, [ATLAS Collaboration] et al., Phys. Lett. B **716**, 1 (2012). [arXiv:1207.7214](https://arxiv.org/abs/1207.7214) [hep-ex]
- S. Chatrchyan, [CMS Collaboration] et al., Phys. Lett. B **716**, 30 (2012). [arXiv:1207.7235](https://arxiv.org/abs/1207.7235) [hep-ex]
- G. Aad, [ATLAS and CMS Collaborations] et al., Phys. Rev. Lett. **114**, 191803 (2015). [arXiv:1503.07589](https://arxiv.org/abs/1503.07589) [hep-ex]
- N. Aghanim et al., [Planck Collaboration] Astron. Astrophys. **641**, A6 (2020). [arXiv:1807.06209](https://arxiv.org/abs/1807.06209) [astro-ph.CO]
- M. Drees, M.M. Nojiri, Phys. Rev. D **47**, 376 (1993). [arXiv:hep-ph/9207234](https://arxiv.org/abs/hep-ph/9207234)
- G.L. Kane, C.F. Kolda, L. Roszkowski, J.D. Wells, Phys. Rev. D **49**, 6173 (1994). [arXiv:hep-ph/9312272](https://arxiv.org/abs/hep-ph/9312272)
- H. Baer, C. Balazs, JCAP **0305**, 006 (2003). [arXiv:hep-ph/0303114](https://arxiv.org/abs/hep-ph/0303114)
- A.B. Lahanas, D.V. Nanopoulos, Phys. Lett. B **568**, 55 (2003). [arXiv:hep-ph/0303130](https://arxiv.org/abs/hep-ph/0303130)

51. U. Chattopadhyay, A. Corsetti, P. Nath, Phys. Rev. D **68**, 035005 (2003). [arXiv:hep-ph/0303201](#)
52. J. Ellis, K.A. Olive, in *Particle Dark Matter*, ed. by G. Bertone, pp. 142–163. [arXiv:1001.3651](#) [astro-ph.CO]
53. J. Ellis, K.A. Olive, Eur. Phys. J. C **72**, 2005 (2012). [arXiv:1202.3262](#) [hep-ph]
54. J. Cao, Z. Heng, D. Li, J.M. Yang, Phys. Lett. B **710**, 665–670 (2012). [arXiv:1112.4391](#) [hep-ph]
55. O. Buchmueller et al., Eur. Phys. J. C **74**(3), 2809 (2014). [arXiv:1312.5233](#) [hep-ph]
56. E.A. Bagnaschi, O. Buchmueller, R. Cavanaugh, M. Citron, A. De Roeck, M.J. Dolan, J.R. Ellis, H. Flücher, S. Heinemeyer, G. Isidori et al., Eur. Phys. J. C **75**, 500 (2015). [arXiv:1508.01173](#) [hep-ph]
57. E. Bagnaschi, H. Bahl, J. Ellis, J. Evans, T. Hahn, S. Heinemeyer, W. Hollik, K. Olive, S. Pasetto, H. Rzehak, I. Sobolev, G. Weiglein, J. Zheng, Eur. Phys. J. C **79**(2), 149 (2019). [arXiv:1810.10905](#) [hep-ph]
58. J.R. Ellis, K.A. Olive, Y. Santoso, V.C. Spanos, Phys. Lett. B **565**, 176 (2003). [arXiv:hep-ph/0303043](#)
59. J. Ellis, F. Luo, K.A. Olive, P. Sandick, Eur. Phys. J. C **73**(4), 2403 (2013). [arXiv:1212.4476](#) [hep-ph]
60. O. Buchmueller, M. Citron, J. Ellis, S. Guha, J. Marrouche, K.A. Olive, K. de Vries, J. Zheng, Eur. Phys. J. C **75**(10), 469 (2015). [Erratum: Eur. Phys. J. C **76**(4), 190 (2016)]. [arXiv:1505.04702](#) [hep-ph]
61. J. Ellis, J.L. Evans, F. Luo, N. Nagata, K.A. Olive, P. Sandick, Eur. Phys. J. C **76**(1), 8 (2016). [arXiv:1509.08838](#) [hep-ph]
62. J. Ellis, J.L. Evans, F. Luo, K.A. Olive, J. Zheng, Eur. Phys. J. C **78**(5), 425 (2018). [arXiv:1801.09855](#) [hep-ph]
63. J. Ellis, J.L. Evans, N. Nagata, K.A. Olive, L. Velasco-Sevilla, Eur. Phys. J. C **80**(4), 332 (2020). [arXiv:1912.04888](#) [hep-ph]
64. S. Heinemeyer, D. Stockinger, G. Weiglein, Nucl. Phys. B **690**, 62–80 (2004). [arXiv:hep-ph/0312264](#)
65. T. Ibrahim, P. Nath, Phys. Rev. D **62**, 015004 (2000)
66. S. Mizuta, D. Ng, M. Yamaguchi, Phys. Lett. B **300**, 96–103 (1993). [arXiv:hep-ph/9210241](#)
67. A. Corsetti, P. Nath, Phys. Rev. D **64**, 125010 (2001). [arXiv:hep-ph/0003186](#)
68. A. Birkedal-Hansen, B.D. Nelson, Phys. Rev. D **64**, 015008 (2001). [arXiv:hep-ph/0102075](#)
69. U. Chattopadhyay, A. Corsetti, P. Nath, Phys. Rev. D **66**, 035003 (2002). [arXiv:hep-ph/0201001](#)
70. V. Bertin, E. Nezri, J. Orloff, JHEP **02**, 046 (2003). [arXiv:hep-ph/0210034](#)
71. A. Birkedal-Hansen, B.D. Nelson, Phys. Rev. D **67**, 095006 (2003). [arXiv:hep-ph/0211071](#)
72. A. Bottino, N. Fornengo, S. Scopel, Phys. Rev. D **67**, 063519 (2003). [arXiv:hep-ph/0212379](#)
73. A. Bottino, F. Donato, N. Fornengo, S. Scopel, Phys. Rev. D **68**, 043506 (2003). [arXiv:hep-ph/0304080](#)
74. U. Chattopadhyay, D.P. Roy, Phys. Rev. D **68**, 033010 (2003). [arXiv:hep-ph/0304108](#)
75. D.G. Cerdeno, C. Munoz, JHEP **10**, 015 (2004). [arXiv:hep-ph/0405057](#)
76. J. Ellis, J.L. Evans, F. Luo, K.A. Olive, JHEP **02**, 071 (2016). [arXiv:1510.03498](#) [hep-ph]
77. H. Baer, A. Mustafayev, S. Profumo, A. Belyaev, X. Tata, Phys. Rev. D **71**, 095008 (2005). [arXiv:hep-ph/0412059](#)
78. H. Baer, A. Mustafayev, S. Profumo, A. Belyaev, X. Tata, JHEP **0507**, 065 (2005). [arXiv:hep-ph/0504001](#)
79. J.R. Ellis, K.A. Olive, P. Sandick, Phys. Rev. D **78**, 075012 (2008). [arXiv:0805.2343](#) [hep-ph]
80. J. Ellis, F. Luo, K.A. Olive, P. Sandick, Eur. Phys. J. C **73**, 2403 (2013). [arXiv:1212.4476](#) [hep-ph]
81. O. Buchmueller et al., Eur. Phys. J. C **74**(6), 2922 (2014). [arXiv:1312.5250](#) [hep-ph]
82. J. Ellis, K. Olive, Y. Santoso, Phys. Lett. B **539**, 107 (2002). [arXiv:hep-ph/0204192](#)
83. J.R. Ellis, T. Falk, K.A. Olive, Y. Santoso, Nucl. Phys. B **652**, 259 (2003). [arXiv:hep-ph/0210205](#)
84. O. Buchmueller et al., Eur. Phys. J. C **74**(12), 3212 (2014). [arXiv:1408.4060](#) [hep-ph]
85. M. Yamaguchi, W. Yin, PTEP **2018**(2), 023B06 (2018). [arXiv:1606.04953](#) [hep-ph]
86. M.A. Ajaib, F. Nasir, [arXiv:2302.02047](#) [hep-ph]
87. J. Ellis, T. Falk, K.A. Olive, Phys. Lett. B **444**, 367 (1998). [arXiv:hep-ph/9810360](#)
88. J. Ellis, T. Falk, K.A. Olive, M. Srednicki, AstroPart. Phys. **13**, 181 (2000). [Erratum-ibid. **15**, 413 (2001)]. [arXiv:hep-ph/9905481](#)
89. R. Arnowitt, B. Dutta, Y. Santoso, Nucl. Phys. B **606**, 59 (2001). [arXiv:hep-ph/0102181](#)
90. M.E. Gómez, G. Lazarides, C. Pallis, Phys. Rev. D **D61**, 123512 (2000). [arXiv:hep-ph/9907261](#)
91. M.E. Gómez, G. Lazarides, C. Pallis, Phys. Lett. B **487**, 313 (2000). [arXiv:hep-ph/0004028](#)
92. M.E. Gómez, G. Lazarides, C. Pallis, Nucl. Phys. B **B638**, 165 (2002). [arXiv:hep-ph/0203131](#)
93. T. Nihei, L. Roszkowski, R. Ruiz de Austri, JHEP **0207**, 024 (2002). [arXiv:hep-ph/0206266](#)
94. M. Citron, J. Ellis, F. Luo, J. Marrouche, K.A. Olive, K.J. de Vries, Phys. Rev. D **87**(3), 036012 (2013). [arXiv:1212.2886](#) [hep-ph]
95. N. Desai, J. Ellis, F. Luo, J. Marrouche, Phys. Rev. D **90**(5), 055031 (2014). [arXiv:1404.5061](#) [hep-ph]
96. M. Chakraborti, S. Heinemeyer, I. Saha, Eur. Phys. J. C **80**(10), 984 (2020). [arXiv:2006.15157](#) [hep-ph]
97. M. Chakraborti, S. Heinemeyer, I. Saha, Eur. Phys. J. C **84**(2), 165 (2024). [arXiv:2308.05723](#) [hep-ph]
98. M.E. Gomez, Q. Shafi, A. Tiwari, C.S. Un, Eur. Phys. J. C **82**(6), 561 (2022). [arXiv:2202.06419](#) [hep-ph]
99. N. Arkani-Hamed, A. Delgado, G.F. Giudice, Nucl. Phys. B **741**, 108–130 (2006). [arXiv:hep-ph/0601041](#)
100. H. Baer, A. Mustafayev, E.K. Park, X. Tata, JCAP **01**, 017 (2007). [arXiv:hep-ph/0611387](#)
101. M. Chakraborti, S. Heinemeyer, I. Saha, Eur. Phys. J. C **81**(12), 1069 (2021). [arXiv:2103.13403](#) [hep-ph]
102. See, for example, C.F. Berger, J.S. Gainer, J.L. Hewett, T.G. Rizzo, JHEP **0902**, 023 (2009). [arXiv:0812.0980](#) [hep-ph]
103. S.S. AbdusSalam, B.C. Allanach, F. Quevedo, F. Feroz, M. Hobson, Phys. Rev. D **81**, 095012 (2010). [arXiv:0904.2548](#) [hep-ph]
104. J.A. Conley, J.S. Gainer, J.L. Hewett, M.P. Le, T.G. Rizzo, Eur. Phys. J. C **71**, 1697 (2011). [arXiv:1009.2539](#) [hep-ph]
105. J.A. Conley, J.S. Gainer, J.L. Hewett, M.P. Le, T.G. Rizzo, [arXiv:1103.1697](#) [hep-ph]
106. B.C. Allanach, A.J. Barr, A. Dafinca, C. Gwenlan, JHEP **1107**, 104 (2011). [arXiv:1105.1024](#) [hep-ph]
107. S. Sekmen, S. Kraml, J. Lykken, F. Moortgat, S. Padhi, L. Pape, M. Pierini, H.B. Prosper et al., JHEP **1202**, 075 (2012). [arXiv:1109.5119](#) [hep-ph]
108. A. Arbey, M. Battaglia, F. Mahmoudi, Eur. Phys. J. C **72**, 1847 (2012). [arXiv:1110.3726](#) [hep-ph]
109. A. Arbey, M. Battaglia, A. Djouadi, F. Mahmoudi, Phys. Lett. B **720**, 153 (2013). [arXiv:1211.4004](#) [hep-ph]
110. M.W. Cahill-Rowley, J.L. Hewett, A. Ismail, T.G. Rizzo, Phys. Rev. D **88**(3), 035002 (2013). [arXiv:1211.1981](#) [hep-ph]
111. C. Streub, G. Bertone, G.J. Besjes, S. Caron, R. Ruiz de Austri, A. Strubig, R. Trotta, JHEP **1409**, 081 (2014). [arXiv:1405.0622](#) [hep-ph]
112. M. Cahill-Rowley, J.L. Hewett, A. Ismail, T.G. Rizzo, Phys. Rev. D **91**(5), 055002 (2015). [arXiv:1407.4130](#) [hep-ph]

113. L. Roszkowski, E.M. Sessolo, A.J. Williams, JHEP **1502**, 014 (2015). [arXiv:1411.5214](https://arxiv.org/abs/1411.5214) [hep-ph]
114. M.E. Cabrera-Catalan, S. Ando, C. Weniger, F. Zandanel, Phys. Rev. D **92**(3), 035018 (2015). [arXiv:1503.00599](https://arxiv.org/abs/1503.00599) [hep-ph]
115. J. Chakraborty, A. Choudhury, S. Mondal, JHEP **07**, 038 (2015). [arXiv:1503.08703](https://arxiv.org/abs/1503.08703) [hep-ph]
116. K.J. de Vries, E.A. Bagnaschi, O. Buchmueller, R. Cavanaugh, M. Citron, A. De Roeck, M.J. Dolan, J.R. Ellis, H. Flücher, S. Heinemeyer et al., Eur. Phys. J. C **75**(9), 422 (2015). [arXiv:1504.03260](https://arxiv.org/abs/1504.03260) [hep-ph]
117. M. Van Beekveld, W. Beenakker, M. Schutten, J. De Wit, SciPost Phys. **11**(3), 049 (2021). [arXiv:2104.03245](https://arxiv.org/abs/2104.03245) [hep-ph]
118. Information about this code is available from K. A. Olive: it contains important contributions from J. Evans, T. Falk, A. Ferstl, G. Ganis, F. Luo, A. Mustafayev, J. McDonald, F. Luo, K.A. Olive, P. Sandick, Y. Santoso, V. Spanos, M. Srednicki, L. Velasco-Sevilla, J. Zheng
119. V. Barger, M.S. Berger, P. Ohmann, Phys. Rev. D **49**, 4908 (1994). [arXiv:hep-ph/9311269](https://arxiv.org/abs/hep-ph/9311269)
120. M. Carena, J. Ellis, A. Pilaftsis, C.E. Wagner, Nucl. Phys. B **586**, 92 (2000). [arXiv:hep-ph/0003180](https://arxiv.org/abs/hep-ph/0003180)
121. S. Heinemeyer, W. Hollik, G. Weiglein, Comput. Phys. Commun. **124**, 76 (2000). [arXiv:hep-ph/9812320](https://arxiv.org/abs/hep-ph/9812320)
122. S. Heinemeyer, W. Hollik, G. Weiglein, Eur. Phys. J. C **9**, 343 (1999). [arXiv:hep-ph/9812472](https://arxiv.org/abs/hep-ph/9812472)
123. G. Degrandi, S. Heinemeyer, W. Hollik, P. Slavich, G. Weiglein, Eur. Phys. J. C **28**, 133 (2003). [arXiv:hep-ph/0212020](https://arxiv.org/abs/hep-ph/0212020)
124. M. Frank et al., JHEP **0702**, 047 (2007). [arXiv:hep-ph/0611326](https://arxiv.org/abs/hep-ph/0611326)
125. T. Hahn, S. Heinemeyer, W. Hollik, H. Rzehak, G. Weiglein, Comput. Phys. Commun. **180**, 1426 (2009)
126. T. Hahn, S. Heinemeyer, W. Hollik, H. Rzehak, G. Weiglein, Phys. Rev. Lett. **112**(14), 141801 (2014). [arXiv:1312.4937](https://arxiv.org/abs/1312.4937) [hep-ph]
127. H. Bahl, W. Hollik, Eur. Phys. J. C **76**(9), 499 (2016). [arXiv:1608.01880](https://arxiv.org/abs/1608.01880) [hep-ph]
128. H. Bahl, S. Heinemeyer, W. Hollik, G. Weiglein, Eur. Phys. J. C **78**(1), 57 (2018). [arXiv:1706.00346](https://arxiv.org/abs/1706.00346) [hep-ph]
129. H. Bahl, T. Hahn, S. Heinemeyer, W. Hollik, S. Pasetto, H. Rzehak, G. Weiglein, Comput. Phys. Commun. **249**, 107099 (2020). [arXiv:1811.09073](https://arxiv.org/abs/1811.09073) [hep-ph]. See <http://www.feynhiggs.de> for updates
130. D. Pierce, A. Papadopoulos, Phys. Rev. D **50**, 565 (1994). [arXiv:hep-ph/9312248](https://arxiv.org/abs/hep-ph/9312248)
131. D. Pierce, A. Papadopoulos, Nucl. Phys. B **430**, 278 (1994). [arXiv:hep-ph/9403240](https://arxiv.org/abs/hep-ph/9403240)
132. D.M. Pierce, J.A. Bagger, K. Matchev, R. Zhang, Nucl. Phys. B **491**, 3 (1997). [arXiv:hep-ph/9606211](https://arxiv.org/abs/hep-ph/9606211)
133. N. Metropolis, A.W. Rosenbluth, M.N. Rosenbluth, A.H. Teller, E. Teller, J. Chem. Phys. **21**, 1087–1092 (1953). <https://doi.org/10.1063/1.1699114>
134. W.K. Hastings, Biometrika **57**, 97–109 (1970). <https://doi.org/10.1093/biomet/57.1.97>
135. LEPSUSYWG, ALEPH, DELPHI, L3 and OPAL Collaborations, LEPSUSYWG/01-03.1 (2001). <https://lepsusy.web.cern.ch/lepsusy/Welcome.html>
136. LEPSUSYWG, ALEPH, DELPHI, L3 and OPAL Collaborations, LEPSUSYWG/02-04.1 (2002). <https://lepsusy.web.cern.ch/lepsusy/Welcome.html>
137. R.L. Workman et al. [Particle Data Group], PTEP **2022**, 083C01 (2022)
138. G. Aad et al. [ATLAS Collaboration], Eur. Phys. J. C **80**(2), 123 (2020). [arXiv:1908.08215](https://arxiv.org/abs/1908.08215) [hep-ex]
139. ATLAS Collaboration, *SUSY August 2023 Summary Plot Update*, ATL-PHYS-PUB-2023-025 (2023), Fig. 15
140. G. Aad et al. [ATLAS Collaboration], Phys. Rev. D **101**(5), 052005 (2020). [arXiv:1911.12606](https://arxiv.org/abs/1911.12606) [hep-ex]
141. J. Ellis, N. Nagata, K.A. Olive, Eur. Phys. J. C **78**(7), 569 (2018). [arXiv:1805.09795](https://arxiv.org/abs/1805.09795) [hep-ph]
142. J.R. Ellis, K.A. Olive, C. Savage, Phys. Rev. D **77**, 065026 (2008). [arXiv:0801.3656](https://arxiv.org/abs/0801.3656) [hep-ph]
143. J. Aalbers et al. [LZ Collaboration], Phys. Rev. Lett. **131**(4), 041002 (2023). [arXiv:2207.03764](https://arxiv.org/abs/2207.03764) [hep-ex]
144. C. Amole et al. [PICO Collaboration], Phys. Rev. D **100**(2), 022001 (2019). [arXiv:1902.04031](https://arxiv.org/abs/1902.04031) [astro-ph.CO]
145. S. Mizuta, M. Yamaguchi, Phys. Lett. B **298**, 120 (1993). [arXiv:hep-ph/9208251](https://arxiv.org/abs/hep-ph/9208251)
146. J. Edsjo, P. Gondolo, Phys. Rev. D **56**, 1879 (1997). [arXiv:hep-ph/9704361](https://arxiv.org/abs/hep-ph/9704361)
147. H. Baer, C. Balazs, A. Belyaev, JHEP **0203**, 042 (2002). [arXiv:hep-ph/0202076](https://arxiv.org/abs/hep-ph/0202076)
148. A. Birkedal-Hansen, E.H. Jeong, JHEP **0302**, 047 (2003). [arXiv:hep-ph/0210041](https://arxiv.org/abs/hep-ph/0210041)
149. J. Edsjo, M. Schelke, P. Ullio, P. Gondolo, JCAP **0304**, 001 (2003). [arXiv:hep-ph/0301106](https://arxiv.org/abs/hep-ph/0301106)
150. A. Sommerfeld, Ann. Phys. **403**, 257 (1931)
151. J. Hisano, S. Matsumoto, M. Nagai, O. Saito, M. Senami, Phys. Lett. B **646**, 34 (2007). [arXiv:hep-ph/0610249](https://arxiv.org/abs/hep-ph/0610249)
152. M. Cirelli, A. Strumia, M. Tamburini, Nucl. Phys. B **787**, 152 (2007). [arXiv:0706.4071](https://arxiv.org/abs/0706.4071) [hep-ph]
153. A. Hryczuk, R. Iengo, P. Ullio, JHEP **1103**, 069 (2011). [arXiv:1010.2172](https://arxiv.org/abs/1010.2172) [hep-ph]
154. M. Beneke, A. Bharucha, F. Dighera, C. Hellmann, A. Hryczuk, S. Recksiegel, P. Ruiz-Femenia, JHEP **1603**, 119 (2016). [arXiv:1601.04718](https://arxiv.org/abs/1601.04718) [hep-ph]
155. E. Bagnaschi, M. Borsato, K. Sakurai, O. Buchmueller, R. Cavanaugh, V. Chobanova, M. Citron, J.C. Costa, A. De Roeck, M.J. Dolan et al., Eur. Phys. J. C **77**(4), 268 (2017). [arXiv:1612.05210](https://arxiv.org/abs/1612.05210) [hep-ph]
156. C.A.J. O'Hare, Phys. Rev. Lett. **127**(25), 251802 (2021). [arXiv:2109.03116](https://arxiv.org/abs/2109.03116) [hep-ph]
157. Internet Movie Database, *Monty Python and the Holy Grail*. <https://www.imdb.com/title/tt0071853/>